

---

# Advancing Graph Convolutional Networks via General Spectral Wavelets

---

Nian Liu<sup>1</sup> Xiaoxin He<sup>1</sup> Thomas Laurent<sup>2</sup> Francesco Di Giovanni<sup>3</sup>  
Michael M. Bronstein<sup>3</sup> Xavier Bresson<sup>1</sup>

{nianliu, xiaoxin, xaviercs}@comp.nus.edu.sg, tlaurent@lmu.edu  
{francesco.di.giovanni, michael.bronstein}@cs.ox.ac.uk

<sup>1</sup>National University of Singapore <sup>2</sup>Loyola Marymount University <sup>3</sup>University of Oxford

## Abstract

Spectral graph convolution, an important tool of data filtering on graphs, relies on two essential decisions; selecting spectral bases for signal transformation and parameterizing the kernel for frequency analysis. While recent techniques mainly focus on standard Fourier transform and vector-valued spectral functions, they fall short in flexibility to describe specific signal distribution for each node, and expressivity of spectral function. In this paper, we present a novel wavelet-based graph convolution network, namely WaveGC, which integrates multi-resolution spectral bases and a matrix-valued filter kernel. Theoretically, we establish that WaveGC can effectively capture and decouple short-range and long-range information, providing superior filtering flexibility, surpassing existing graph convolutional networks and graph Transformers (GTs). To instantiate WaveGC, we introduce a novel technique for learning general graph wavelets by separately combining odd and even terms of Chebyshev polynomials. This approach strictly satisfies wavelet admissibility criteria. Our numerical experiments showcase the capabilities of the new network. By replacing the Transformer part in existing architectures with WaveGC, we consistently observe improvements in both short-range and long-range tasks. This underscores the effectiveness of the proposed model in handling different scenarios. Our code is available at <https://github.com/liun-online/WaveGC>.

## 1 Introduction

Spectral graph theory (SGT) [10], which enables analysis and learning on graph data, has firmly established itself as a pivotal methodology in graph machine learning. A significant milestone in SGT is the generalization of the convolution operation to graphs, as convolution for grid-structured data, i.e. sequences and images, has demonstrated remarkable success [35, 23, 33]. Significant research interests in graph convolution revolve around two key factors: (1) *designing diverse bases for spectral transform*, and (2) *parameterizing powerful graph kernel*. For (1), the commonly used graph Fourier basis, consisting of the eigenvectors of the graph Laplacian [51], stands as a prevalent choice. However, graph wavelets [20] offer enhanced expressiveness by constructing adaptable bases. For (2), classic approaches involve diagonalizing the kernel with fully free parameters [5] or employing various polynomial approximations such as Chebyshev [11] and Cayley [37] polynomials. Additionally, convolution with a matrix-valued kernel serves as the spectral function of Transformer [54] under the shift-invariant condition [39, 18].

Despite the existence of techniques in each aspect, the integration of these two lines into a unified framework remains challenging, impeding the full potential of graph convolution. In an effort to unravel this challenge, we introduce a novel operation — **Wavelet-based Graph Convolution**

(WaveGC), which seamlessly incorporates both spectral basis and kernel considerations. In terms of spectral basis design, WaveGC is built upon graph wavelets, allowing it to capture information across the entire graph through a multi-resolution approach from highly adaptive construction of multiple graph wavelet bases. For filter parameterization, we opt for a matrix-valued spectral kernel with weight-sharing. Beyond adjusting diagonal frequencies, the matrix-valued kernel offers greater flexibility to spectral filtering, thanks to its larger parameter space.

To comprehensively explore WaveGC, we theoretically analyse and assess its information-capturing capabilities. In contrast to the one-hop message-passing framework of basic graph convolution, WaveGC is demonstrated to exhibit both significantly larger and smaller receptive fields concurrently, achieved through the manipulation of scales. Previous graph wavelet theory [20] only verifies the localization in small scale limit. Instead, our proof is complete as it covers both extremely small and large scales from the perspective of information mixing [12]. Moreover, our proof also implies that WaveGC is capable of simultaneously capturing both short-range and long-range information for each node, akin to (graph) Transformers, which facilitate global node interaction. Remarkably, WaveGC can distinguish information across diverse distances, thereby extending its flexibility beyond the scope of traditional Transformers.

To implement WaveGC, a critical step lies in constructing graph wavelet bases that satisfy two fundamental criteria: (1) meeting the wavelet admissibility criteria [42] and (2) showing adaptability to different graphs. Existing designs of graph wavelets face limitations, with some falling short in ensuring the criteria [61, 63], while others having fixed wavelet forms, lacking adaptability [66, 9]. To address these limitations, we propose an innovative and general implementation of graph wavelets. Our solution involves *approximating scaling function basis and multiple wavelet bases using odd and even terms of Chebyshev polynomials, respectively*. This approach is inspired by our observation that, after a certain transformation, even terms of Chebyshev polynomials strictly satisfy the admissibility criteria, while odd terms supplement direct current signals. Through the combination of these terms via learnable coefficients, we aim to theoretically approximate scaling function and multiple wavelets with arbitrary complexity and flexibility. Our contributions are:

- We introduce an innovative graph convolution via wavelets, WaveGC, which integrates multi-resolution spectral bases and a matrix-valued convolution kernel, unlocking new potentials in graph convolution.
- We theoretically reveal that WaveGC can capture and distinguish the information from different distances, surpassing conventional graph convolutions and GTs.
- We pioneer a general implementation of learnable graph wavelets, employing odd terms and even terms of Chebyshev polynomials individually. This implementation strictly satisfies the wavelet admissibility criteria.
- Integrating WaveGC into three successful GTs as base models, our approach consistently outperforms base methods on both short-range and long-range tasks, achieving up to 26.20% improvement on CoraFull and 9.21% on VOC datasets.

## 2 Preliminaries

An undirected graph can be presented as  $\mathcal{G} = (\mathcal{V}, E)$ , where  $\mathcal{V}$  is the set of  $N$  nodes and  $E \subseteq \mathcal{V} \times \mathcal{V}$  is the set of edges. The adjacency matrix of this graph is  $\mathbf{A} \in \{0, 1\}^{N \times N}$ , where  $\mathbf{A}_{ij} \in \{0, 1\}$  denotes the relation between nodes  $i$  and  $j$  in  $\mathcal{V}$ . The degree matrix is  $\mathbf{D} = \text{diag}(d_1, \dots, d_N) \in \mathbb{R}^{N \times N}$ , where  $d_i = \sum_{j \in \mathcal{V}} \mathbf{A}_{ij}$  is the degree of node  $i \in \mathcal{V}$ . The node feature matrix is  $\mathbf{X} = [x_1, x_2, \dots, x_N] \in \mathbb{R}^{N \times d_0}$ , where  $x_i$  is a  $d_0$  dimensional feature vector of node  $i \in \mathcal{V}$ . Let  $\hat{\mathbf{A}} = \mathbf{D}^{-\frac{1}{2}} \mathbf{A} \mathbf{D}^{-\frac{1}{2}}$  be the symmetric normalized adjacency matrix, then  $\hat{\mathbf{L}} = \mathbf{I}_n - \hat{\mathbf{A}} = \mathbf{D}^{-\frac{1}{2}} (\mathbf{D} - \mathbf{A}) \mathbf{D}^{-\frac{1}{2}}$  is the symmetric normalized graph Laplacian. With eigen-decomposition,  $\hat{\mathbf{L}} = \mathbf{U} \mathbf{\Lambda} \mathbf{U}^\top$ , where  $\mathbf{\Lambda} = \text{diag}(\lambda_1, \dots, \lambda_N) \in \mathbb{R}^{N \times N}$  and  $\mathbf{U} = [\mathbf{u}_1^\top, \dots, \mathbf{u}_N^\top] \in \mathbb{R}^{N \times N}$  are the eigenvalues and eigenvectors of  $\hat{\mathbf{L}}$ , respectively. Given a signal  $f \in \mathbb{R}^N$  on  $\mathcal{G}$ , the graph Fourier transform [51] is defined as  $\hat{f} = \mathbf{U}^\top f \in \mathbb{R}^N$ , and its inverse is  $f = \mathbf{U} \hat{f} \in \mathbb{R}^N$ .

**Spectral graph wavelet transform (SGWT).** Hammond et al. [20] redefine the wavelet basis [42] on vertices in the spectral graph domain. Specifically, the SGWT is composed of three components: (1) *Unit wavelet basis*, denoted as  $\Psi$  such that  $\Psi = g(\hat{\mathbf{L}}) = \mathbf{U} g(\mathbf{\Lambda}) \mathbf{U}^\top$ , where  $g$  acts as a band-pass

filter  $g : \mathbb{R}^+ \rightarrow \mathbb{R}^+$  meeting the following *wavelet admissibility criteria* [42]:

$$C_\Psi = \int_{-\infty}^{\infty} \frac{|g(\lambda)|^2}{|\lambda|} d\lambda < \infty. \quad (1)$$

To meet this requirement,  $g(\lambda = 0) = 0$  and  $\lim_{\lambda \rightarrow \infty} g(\lambda) = 0$  are two essential prerequisites. (2) *Spatial scales*, a series of positive real values  $\{s_j\}$  where distinct values of  $s_j$  with  $\Psi_{s_j} = \mathbf{U}g(s_j\mathbf{\Lambda})\mathbf{U}^\top$  can control different size of neighbors. (3) *Scaling function basis*, denoted as  $\Phi$  such that  $\Phi = \mathbf{U}h(\lambda)\mathbf{U}^\top$ . Here, the function of  $h : \mathbb{R}^+ \rightarrow \mathbb{R}^+$  is to supplement direct current (DC) signals at  $\lambda = 0$ , which is omitted by all wavelets  $g(s_j\lambda)$  since  $g(0) = 0$ . Next, given a signal  $f \in \mathbb{R}^N$ , the formal SGWT [20] is:

$$W_f(s_j) = \Psi_{s_j} f = \mathbf{U}g(s_j\mathbf{\Lambda})\mathbf{U}^\top f \in \mathbb{R}^N, \quad (2)$$

where  $W_f(s_j)$  is the wavelet coefficients of  $f$  under scale  $s_j$ . Similarly, scaling function coefficients are given by  $S_f = \Phi f = \mathbf{U}h(\mathbf{\Lambda})\mathbf{U}^\top f \in \mathbb{R}^N$ . Let  $G(\lambda) = h(\lambda)^2 + \sum_j g(s_j\lambda)^2$ , then if  $G(\lambda) \equiv 1, \forall \lambda \in \mathbf{\Lambda}$ , the constructed graph wavelets are known as *tight frames*, which guarantee energy conservation of the given signal between the original and the transformed domains [52]. More spectral graph wavelets are introduced in Appendix E.

### 3 From Graph Convolution to Graph Wavelets

Spectral graph convolution is a fundamental operation in the field of graph signal processing [51]. Specifically, given a signal matrix (or node features)  $\mathbf{X} \in \mathbb{R}^{N \times d}$  on graph  $\mathcal{G}$ , the spectral filtering of this signal is defined with a kernel  $\kappa \in \mathbb{R}^{N \times N}$  by the convolution theorem [1]:

$$\kappa *_G \mathbf{X} = \mathcal{F}^{-1}(\mathcal{F}(\kappa) \cdot \mathcal{F}(\mathbf{X})) \in \mathbb{R}^{N \times N}, \quad (3)$$

where  $\cdot$  is the matrix multiplication operator,  $\mathcal{F}(\cdot)$  and  $\mathcal{F}^{-1}(\cdot)$  are the spectral transform (e.g., graph Fourier transform [5]) and corresponding inverse transform, respectively. To design a new convolution operation, two critical choices must be considered in Eq. (3): 1) the parameterization of the kernel  $\kappa$  and 2) the selection of the transform  $\mathcal{F}$ .

#### 3.1 Matrix-valued kernel via sharing weight

Spectral function  $\mathcal{F}(\kappa)$  in Eq. (3) is usually parameterized with  $\theta$ . Let us consider two cases:

**1) Vector-valued function.**  $\mathcal{F}(\kappa) = \mathcal{F}_\theta(\mathbf{\Lambda})$  is parameterized diagonally, where diagonal elements are adjustments on the spectrum of the graph  $\mathcal{G}$ . Bruna et al. [5] directly set  $\mathcal{F}_\theta(\mathbf{\Lambda}) = \text{diag}(\theta)$ , fully free to optimize. ChebNet [11] further sets  $\mathcal{F}_\theta(\mathbf{\Lambda}) = \sum_k \theta_k T_k(\mathbf{\Lambda})$ , where  $T_k(\cdot)$  is the  $k$ -th term of Chebyshev polynomials. Most spectral graph neural networks adhere to learning spectral functions as a linear combination of basis functions derived from the graph spectrum, s.a. CayleyNet [37].

**2) Matrix-valued function.** If  $\kappa$  is parameterized as an matrix-valued kernel, then Eq. (3) is the formula of shift-invariant Transformers [39]. Specifically, the vanilla Transformer [54] is given as:

$$\mathbf{H}^{(l+1)} = \text{softmax} \left( \frac{\mathbf{H}^{(l)} \mathbf{W}_q (\mathbf{H}^{(l)} \mathbf{W}_k)^\top}{\sqrt{d}} \right) \mathbf{H}^{(l)} \mathbf{W}_v, \quad (4)$$

where  $\mathbf{H}^{(l)}, \mathbf{H}^{(l+1)} \in \mathbb{R}^{N \times d}$  are node embeddings from  $l$ -th and  $(l+1)$ -th layers, and  $\{\mathbf{W}_q, \mathbf{W}_k, \mathbf{W}_v\} \in \mathbb{R}^{d \times d}$  are the query, key, and value learnable matrices. Viewing the Transformer through the kernel technique, the attention matrix can be regarded as an asymmetric, shift-invariant kernel denoted as  $R_\theta \in \mathbb{R}^{N \times d \times d}$  [53, 39]. Then, the spectral function of Eq. (4) is:

$$\mathbf{H}^{(l+1)} = \mathcal{F}^{-1}(R_\theta \cdot \mathcal{F}(\mathbf{H}^{(l)})) \in \mathbb{R}^{N \times d}, \quad (5)$$

where  $R_\theta$  is fully parameterized as a neural network. Detailed derivations are given in Appendix B.

In this paper, we express  $\mathcal{F}(\kappa)$  in a matrix-valued form, since a powerful kernel with more parameters provides enough flexibility to adjust itself. Additionally, the experimental evidence in Section 6.2 shows the superiority of matrix-valued kernel against vector-valued one. Notably, the number of parameters in  $R_\theta^{N \times d \times d}$  is quite important, particularly for large-scale graphs with a large value of  $N$ .

To efficiently model  $R_\theta$ , we adopt parameter sharing among all frequency modes, employing only one Multi-Layer Perceptron (MLP). This results in a significant reduction of parameters in  $R_\theta$  from  $N \times d \times d$  to  $d \times d$ . Eq. (5) becomes:

$$\mathbf{H}^{(l+1)} = \mathcal{F}^{-1}(\sigma(\mathcal{F}(\mathbf{H}^{(l)})\mathbf{W}_\kappa^{(l)})) \in \mathbb{R}^{N \times d}, \quad (6)$$

where  $\mathbf{W}_\kappa^{(l)}$  contains learnable weight and bias for neural network  $\mathcal{F}(\kappa)$  at  $l$ -th layer, and  $\sigma$  is the activation function. For traditional point-wise vector-valued kernel, each frequency is independently scaled by one specific coefficient. Instead, our approach allows various frequency modes to interact, allowing them to collaboratively determine the optimal signal filtering strategy. Moreover, this sharing decreases the number of learnable parameters, and consequentially alleviates the risk of over-fitting caused by non-sharing, as in Section 6.2. An alternative method is presented in AFNO [18], introducing a similar technique that offers improved efficiency but with a more intricate design.

### 3.2 General spectral wavelet via Chebyshev decomposition

For the selection of the spectral transform  $\mathcal{F}$  and its inverse  $\mathcal{F}^{-1}$ , it can be tailored to the specific nature of data. For set data, the Dirac Delta function [44] is employed, while the fast Fourier Transform (FFT) proves efficient for both sequences [39] and grids [18]. In the context of graphs, the Fourier transform ( $\mathcal{F} \rightarrow \mathbf{U}^\top$ ) emerges as one classical candidate. However, some inherent flaws limit the expressiveness of Fourier bases. (1) Standard graph Fourier bases, represented by one fixed matrix  $\mathbf{U}^\top$ , maintain a constant resolution and fixed frequency modes. (2) Fourier transform lacks the adaptability to be further optimized according to different datasets and tasks. Therefore, *multiple resolution* and *adaptability* are two prerequisites for the design of an advanced base.

Notably, wavelet base is able to conform the above two demands, and hence offers enhanced expressiveness compared to Fourier base. For the resolution, the use of different scales  $s_j$  allows wavelet to analyze detailed components of a signal at different granularity. More importantly, due to its strong spatial localization [20], each wavelet corresponds to a signal diffused away from a central node [61]. Therefore, these scales also control varying receptive fields in spatial space, which enables the simultaneous fusion of short- and long-range information. For the adaptability, graph wavelets offer the flexibility to adjust the shapes of wavelets and scaling function. These components can be collaboratively optimized for the alignment of basis characteristics with different datasets, potentially enhancing generalization performance.

Next, we need to determine the form of the scaling function basis  $\Phi = \mathbf{U}h(\mathbf{\Lambda})\mathbf{U}^\top$ , the unit wavelet basis  $\Psi = \mathbf{U}g(\mathbf{\Lambda})\mathbf{U}^\top$ , and the scales  $s_j$ . The forms of  $h$  and  $g$  are expected to be expressive enough and easily available. Concurrently,  $g$  should strictly satisfy the wavelet admissibility criteria, i.e., Eq. (1), and  $h$  should complementarily provide DC signals. To achieve this target, we *separately introduce odd terms and even terms from Chebyshev polynomials [20]* into the approximation of  $h$  and  $g$ . Please recall that the Chebyshev polynomial  $T_k(y)$  of order  $k$  may be computed by the stable recurrence relation  $T_k(y) = 2yT_{k-1}(y) - T_{k-2}(y)$  with  $T_0 = 1$  and  $T_1 = y$ . After the following transform, we surprisingly observe that these transformed terms match all above expectations:

$$T_k(y) \rightarrow 1/2 \cdot (-T_k(y-1) + 1). \quad (7)$$

To give a more intuitive illustration, we present the spectra of first several Chebyshev polynomials before and after the transform in Fig. 1 (a), where the set of odd and even terms after the transform are denoted as  $\{T_i^o\}$  and  $\{T_i^e\}$ , respectively. From the figure,  $g(\lambda = 0) \equiv 0$  for all  $\{T_i^e\}$ , and  $h(\lambda = 0) \equiv 1$  for all  $\{T_i^o\}$ . Consequentially,  $\{T_i^e\}$  and  $\{T_i^o\}$  strictly meet the criteria and naturally serve as the basis of unit wavelet and scaling function. Moreover, not only can we easily get each Chebyshev term via iteration, but the constructed wavelet is arbitrarily expressive because of the combination of as many terms as needed. Given  $\{T_i^e\}$  and  $\{T_i^o\}$ , all we need to do is just to learn the coefficients to form the corresponding  $g(\lambda)$  and  $h(\lambda)$ :

$$g(\mathbf{\Lambda}) = \sum_i^\rho a_i T_i^e(\mathbf{\Lambda}) \in \mathbb{R}^{N \times N}, \quad h(\mathbf{\Lambda}) = \sum_i^\rho b_i T_i^o(\mathbf{\Lambda}) \in \mathbb{R}^{N \times N}, \quad (8)$$

where  $\rho$  is the number of truncated terms,  $\tilde{\mathbf{a}} = (a_1, a_2, \dots, a_n) \in \mathbb{R}^{1 \times n}$  and  $\tilde{\mathbf{b}} = (b_1, b_2, \dots, b_n) \in \mathbb{R}^{1 \times n}$  represent two learnable coefficient vectors as follows:

$$\tilde{\mathbf{a}} = \text{Mean}(\mathbf{W}_a \hat{\mathbf{Z}} + \mathbf{b}_a), \quad \tilde{\mathbf{b}} = \text{Mean}(\mathbf{W}_b \hat{\mathbf{Z}} + \mathbf{b}_b), \quad (9)$$

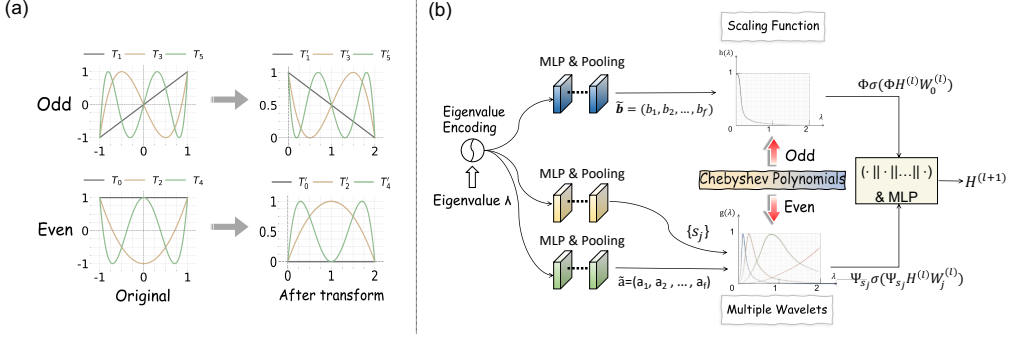


Figure 1: (a) An illustration of Chebyshev polynomials before and after the given transform. In this representation, we distinguish odd and even terms, presenting only the first three terms for each. (b) An overview of our proposed WaveGC.

where  $\{\mathbf{W}_a, \mathbf{W}_b\} \in \mathbb{R}^{d \times n}$  and  $\{\mathbf{b}_a, \mathbf{b}_b\} \in \mathbb{R}^{1 \times n}$  are learnable parameters, and  $\hat{\mathbf{Z}}$  is the eigenvalue embedding composed by the module in [3]. Further details can be found in Appendix C. Similarly, we can learn the scales  $\tilde{\mathbf{s}} = (s_1, s_2, \dots, s_J)$  in the same way:

$$\tilde{\mathbf{s}} = \sigma(\text{Mean}(\mathbf{W}_s \hat{\mathbf{Z}} + \mathbf{b}_s)) \cdot \bar{\mathbf{s}} \in \mathbb{R}^{1 \times J}, \quad (10)$$

where  $\sigma$  is sigmoid function,  $\mathbf{W}_s \in \mathbb{R}^{d \times J}$  and  $\mathbf{b}_s \in \mathbb{R}^{1 \times J}$  are learnable parameters, and  $\bar{\mathbf{s}} = (\bar{s}_1, \bar{s}_2, \dots, \bar{s}_J)$  is a pre-defined vector to control the size of  $\tilde{\mathbf{s}}$ . Please note that for  $g(\Lambda)$  and  $h(\Lambda)$  in Eq. (8), we only keep their spectra within  $\lambda \in [0, 2]$ , since this interval matches the definition of Chebyshev bases [20] before transform.

### 3.3 Wavelet-based Graph Convolution

Until now, we have elaborated the proposed advancements on kernel and bases, and now discuss how to integrate these two aspects. Provided that we have  $J$  wavelet  $\{\Psi_{s_j}\}_{j=1}^J$  and one scaling function  $\Phi$  constructed via the above Chebyshev decomposition,  $\mathcal{F} : \mathbb{R}^{N \times d} \rightarrow \mathbb{R}^{N(J+1) \times d}$  in Eq. (3) is the stack of transforms from each component:

$$\mathcal{F}(\mathbf{H}^{(l)}) = \mathbf{T}\mathbf{H}^{(l)} = ((\Phi \mathbf{H}^{(l)})^\top || (\Psi_{s_1} \mathbf{H}^{(l)})^\top || \dots || (\Psi_{s_J} \mathbf{H}^{(l)})^\top)^\top \in \mathbb{R}^{N(J+1) \times d}, \quad (11)$$

where  $\mathbf{T} = (\Phi^\top || \Psi_{s_1}^\top || \dots || \Psi_{s_J}^\top)^\top$  is the overall transform and  $||$  means concatenation. Next, we check if the inverse  $\mathcal{F}^{-1}$  exists. Considering  $\mathbf{T}$  is not a square matrix,  $\mathcal{F}^{-1}$  should be its pseudo-inverse as  $(\mathbf{T}^\top \mathbf{T})^{-1} \mathbf{T}^\top$ , where  $\mathbf{T}^\top \mathbf{T} = \Phi \Phi^\top + \sum_{j=1}^J \Psi_{s_j} \Psi_{s_j}^\top = \mathbf{U}[h(\lambda)^2 + \sum_{j=1}^J g(s_j \lambda)^2] \mathbf{U}^\top$ . Ideally, if  $\mathbf{T}$  is imposed as **tight frames**, then  $h(\lambda)^2 + \sum_{j=1}^J g(s_j \lambda)^2 = \mathbf{I}$  [36], and  $\mathbf{T}^\top \mathbf{T} = \mathbf{U} \mathbf{U}^\top = \mathbf{I}$ . In this case,  $\mathcal{F}^{-1} = (\mathbf{T}^\top \mathbf{T})^{-1} \mathbf{T}^\top = \mathbf{T}^\top$ , and Eq. (3) becomes:

$$\mathbf{H}^{(l+1)} = \mathbf{T}^\top (\mathcal{F}(\boldsymbol{\kappa}) \cdot \mathbf{T}\mathbf{H}^{(l)}) = \Phi(\mathcal{F}_0(\boldsymbol{\kappa}) \cdot \Phi \mathbf{H}^{(l)}) + \sum_{j=1}^J \Psi_{s_j}(\mathcal{F}_j(\boldsymbol{\kappa}) \cdot \Psi_{s_j} \mathbf{H}^{(l)}) \in \mathbb{R}^{N \times d}, \quad (12)$$

where we separate  $\mathcal{F}(\boldsymbol{\kappa})$  into  $\{\mathcal{F}_j(\boldsymbol{\kappa})\}_{j=0}^J$ , each of which is assigned to a transform component.

**How to guarantee tight frames?** From above derivations, *tight frames* is a key for the simplification of inverse  $\mathcal{F}^{-1}$  in Eq. (12). This can be guaranteed by  $l_2$  norm on the above constructed wavelets and scaling function. For each eigenvalue  $\lambda \in \Lambda$ , we have  $v^2 = h(\lambda)^2 + \sum_{j=1}^J g(s_j \lambda)^2$ ,  $\tilde{h}(\lambda) = h(\lambda)/v$ ,  $\tilde{g}(s_j \lambda) = g(s_j \lambda)/v$ . Then,  $G(\Lambda) = \tilde{h}(\Lambda)^2 + \sum_{j=1}^J \tilde{g}(s_j \Lambda)^2 = \mathbf{I}$  forms tight frames (Section 2). Thus, while the pseudo-inverse must theoretically exist, we can circumvent the necessity of explicitly calculating the pseudo-inverse.

Resembling the multi-head attention [54], we treat each wavelet transform as a ‘‘wavelet head’’, and concatenate them rather than sum them to get  $\mathbf{H}^{(l+1)} \in \mathbb{R}^{N \times d}$ :

$$\mathbf{H}^{(l+1)} = \text{MLP} \left( \Phi(\mathcal{F}_0(\boldsymbol{\kappa}) \cdot \Phi \mathbf{H}^{(l)}) || \Psi_{s_1}(\mathcal{F}_1(\boldsymbol{\kappa}) \cdot \Psi_{s_1} \mathbf{H}^{(l)}) || \dots || \Psi_{s_J}(\mathcal{F}_J(\boldsymbol{\kappa}) \cdot \Psi_{s_J} \mathbf{H}^{(l)}) \right), \quad (13)$$

Table 1: Comparison between classical graph convolution and WaveGC.

	Classical Graph Convolution	WaveGC
Formula	$\sigma(\mathcal{U}\mathcal{F}_\theta(\mathbf{\Lambda})\mathcal{U}^\top\mathbf{H}\mathbf{W})$	$\text{MLP}(\Phi\sigma(\Phi\mathbf{H}\mathbf{W}_0) \parallel \Psi_{s_1}\sigma(\Psi_{s_1}\mathbf{H}\mathbf{W}_1))$
Kernel	$\mathcal{F}_\theta(\mathbf{\Lambda})$	$\sigma(\bullet\mathbf{W}_0) / \sigma(\bullet\mathbf{W}_1)$
Bases	$\mathcal{U}^\top$	$\Phi / \Psi_{s_1}$
Feature transformation	$\sigma(\bullet\mathbf{W})$	$\text{MLP}()$

where an outermost MLP increases the flexibility. Finally, combining Eq. (13) and (6), we obtain our model WaveGC, i.e. a new implementation of graph convolution operation based on wavelets:

$$\mathbf{H}^{(l+1)} = \text{MLP}\left(\Phi\sigma(\Phi\mathbf{H}^{(l)}\mathbf{W}_0^{(l)}) \parallel \Psi_{s_1}\sigma(\Psi_{s_1}\mathbf{H}^{(l)}\mathbf{W}_1^{(l)}) \parallel \dots \parallel \Psi_{s_J}\sigma(\Psi_{s_J}\mathbf{H}^{(l)}\mathbf{W}_J^{(l)})\right) \in \mathbb{R}^{N \times d}. \quad (14)$$

Fig. 1 (b) presents the whole framework. For a better understanding, we compare classical graph convolution and WaveGC in Table. 1, where WaveGC contains only one wavelet for simplicity.

## 4 Theoretical Properties of WaveGC

Traditionally, wavelet is notable for its diverse receptive fields because of varying scales [42]. For graph wavelet, Hammond et al. [20] were the first to prove the localization when scale  $s \rightarrow 0$ , but did not discuss the long-range case when  $s \rightarrow \infty$ . We further augment this discussion and demonstrate the effectiveness of the proposed WaveGC in capturing both short- and long-range information. Intuitively, a model’s ability to integrate global information enables the reception and mixing of messages from distant nodes. Conversely, a model with a limited receptive field can only effectively mix local messages. Hence, assessing the degree of information ‘mixing’ becomes a key property. For this reason, we focus on the concept of *maximal mixing*, defined as follows:

**Definition 4.1. (Maximal mixing)** [12]. *For a twice differentiable graph-function  $y_G$  of node features  $x_i$ , the maximal mixing induced by  $y_G$  among the features  $x_a$  and  $x_b$  with nodes  $a, b$  is*

$$\text{mix}_{y_G}(a, b) = \max_{x_i} \max_{1 \leq \alpha, \beta \leq d} \left| \frac{\partial^2 y_G(\mathbf{X})}{\partial x_a^\alpha \partial x_b^\beta} \right|. \quad (15)$$

This definition is established in the context of graph-level task, and  $y_G$  is the final output of an end-to-end framework, comprising the primary model and a readout function (e.g., mean, max) applied over the last layer.  $\alpha$  and  $\beta$  represent two entries of the  $d$ -dimensional features  $x_a$  and  $x_b$ .

Next, we employ ‘maximal mixing’ on the WaveGC. For simplicity, we only consider one wavelet basis without inverse transform in Eq. (14), i.e.  $\sigma(\Psi_s\mathbf{H}^{(l)}\mathbf{W}_s^{(l)})$ . Let  $\Psi_s = \mathcal{U}g(s\mathbf{\Lambda})\mathcal{U}^\top$ , and further assume  $g$  is smooth enough at  $\lambda = 0$ :

**Assumption 4.2.** Given a large even number  $K > 0$ , suppose  $g$  is  $K + 1$  times continuously differentiable on  $[0, 2]$  and satisfies  $g(0) = 0, g^{(r)}(0) = 0$  for all  $r < K$ , and  $g^{(K)}(0) = C > 0$ .

With this assumption, we have the following theorem to compare  $\sigma(\Psi_s\mathbf{H}^{(l)}\mathbf{W}_s^{(l)})$  and one-hop message passing  $\sigma(\mathbf{A}\mathbf{H}^{(l)}\mathbf{W}_s^{(l)})$ :

**Theorem 4.3 (Short-range and long-range receptive fields).** *Given two random nodes  $a$  and  $b$ , if the depths  $m_\Psi$  and  $m_A$  are necessary for  $\sigma(\Psi_s\mathbf{H}^{(l)}\mathbf{W}_s^{(l)})$  and  $\sigma(\mathbf{A}\mathbf{H}^{(l)}\mathbf{W}_s^{(l)})$  to induce the same amount of mixing  $\text{mix}_{y_G}(b, a)$ , then the lower bounds of  $m_\Psi$  and  $m_A$ , i.e.  $L_{m_\Psi}$  and  $L_{m_A}$ , approximately satisfy the following relation when scale  $s \rightarrow \infty$ :*

$$L_{m_\Psi} \approx \frac{2}{K}L_{m_A} - \frac{2|E|}{K\sqrt{d_a d_b}} \frac{\text{mix}_{y_G}(b, a)}{\gamma}. \quad (16)$$

Or, if  $s \rightarrow 0$ , the relation becomes:

$$L_{m_\Psi} \approx \frac{2}{K}L_{m_A} + \frac{2|E|}{K\sqrt{d_a d_b}} \frac{\text{mix}_{y_G}(b, a)}{\gamma} \cdot \frac{1}{(\alpha^2 s^{2K})^{m_\Psi}}, \quad (17)$$

where  $d_a$  and  $d_b$  are degrees of two nodes, and  $\alpha = \frac{C \cdot 2^K (K+1)}{K!}$ .  $\gamma = \sqrt{\frac{d_{max}}{d_{min}}}$ , where  $d_{max}/d_{min}$  is the maximum / minimum degree in the graph.

The proof is provided in Appendix A.3. From Eq.(16), we see that if  $s \rightarrow \infty$ ,  $\Psi_s$  will achieve the same degree of node mixing as one-hop message passing but with much less propagation. In other words, a single-layer  $\Psi_s$  is able to access longer-range information than one-hop message passing. Conversely, if  $s \rightarrow 0$ , the second term on the right-hand side of Eq. (17) will be large, requiring  $\Psi_s$  to propagate more layers to mix nodes. Consequently,  $\Psi_s$  exclusively receives shorter-range information than one-hop message passing in this scenario. To conclude,  $\Psi_s$  presents the short- and long-range characteristics of WaveGC.

## 5 Why do we need decomposition?

As shown in Fig. 1 (a), odd and even terms of Chebyshev polynomials meet the requirements on constructing wavelet after decomposition and transform. Additionally, each term is apt to be obtained according to the iteration formula, while infinite number of terms guarantee the expressiveness of the final composed wavelet. Next, we compare our decomposition solution with other related techniques:

- *Constructing wavelet via Chebyshev polynomials.* Both SGWT [20] and GWNN [61] firstly fix the shape of wavelets as cubic spline or exponential, followed by the approximation via Chebyshev polynomials. DEFT [2] employs an MLP or GNN network to learn the coefficients for Chebyshev bases. Comprehensively, the constructed wavelets from GWNN and DEFT fail to meet the wavelet admissible criteria because they impose no constraints to guarantee this point. SGWT fails to learn more flexible and expressive wavelet to better suit the dataset and task at hand.
- *Learnable graph bases.* If we uniformly learn the coefficients for all Chebyshev terms without decomposition, WaveGC degrades to a variant similar to ChebNet [11]. However, mixture rather than decomposition blends the signals from different ranges, and the final spatial ranges cannot be precisely predicted and controlled. ChebNetII [21], reducing the Runge phenomenon via interpolation, confronts the same problem. Both JacobiConv [56] and OptBasisGNN [19] emphasize the orthogonality of bases, but fail to manage multiple ranges information in spatial domain.

We provide numerical comparison and spectral visualization in section 6.3 for WaveGC against these related studies. In addition, although both WaveGC and Transformers can handle various node interaction ranges, the former adaptively learns which range must be emphasized, whereas the latter mixes short- and long-range information together without distinction. Thus, WaveGC surpasses Transformers in controlling distance based information.

## 6 Numerical Experiments

In this section, we evaluate the performance of WaveGC on both short-range and long-range benchmarks using the following datasets: (1) *Datasets for short-range tasks:* CS, Photo, Computer and CoraFull from the PyTorch Geometric (PyG) [15], and one large-size graph, i.e. ogbn-arxiv from Open Graph Benchmark (OGB) [25] (2) *Datasets for long-range tasks:* PascalVOC-SP (VOC), PCQM-Contact (PCQM), COCO-SP (COCO), Peptides-func (Pf) and Peptides-struct (Ps) from LRGB [14]. Please refer to Appendix D.2 for details of datasets.

Our aim is to mainly compare WaveGC and graph Transformers on capturing both short- and long-range information. Consequently, we replace the Transformer component in base models with WaveGC, while keeping the remaining components unchanged. The base models are Transformer [54], SAN [32], and GraphGPS [47] because of the presence of the vanilla Transformer architecture in these three methods. Detailed descriptions of Transformer, SAN, and GraphGPS can be found in Appendix D.7. Additionally, we compare our method with other state-of-the-art models tailored to specific scenarios. Please refer to Appendix D.1 for implementation details.

### 6.1 Benchmarking WaveGC

For short-range (S) datasets, we follow the settings from [7]. For ogbn-arxiv, we use the public splits in OGB [25]. For long-range datasets, we adhere to the experimental configurations outlined in [14]. (1) The results for comparing with base models are presented in Table 2. WaveGC consistently enhances the performance of base models across all datasets. (2) The results of the comparison with other SOTA models are shown in Table 3 and 4. Remarkably, our WaveGC demonstrates competitive performance and achieves the best results on CS, Photo, ogbn-arxiv, VOC, COCO and Pf, as well

as securing the second position on Computer and PCQM. In the experiments conducted on the five short-range datasets, the model is required to prioritize local information, while the five long-range datasets necessitate the handling of distant interactions. The results clearly demonstrate that the proposed WaveGC consistently outperforms traditional graph convolutions and GTs in effectively aggregating both local and long-range information.

Table 2: Quantified results on short-range (S) and long-range (L) datasets compared to base models.

Model	CS (S)	Photo (S)	Computer (S)	CoraFull (S)	ogbn-arxiv (S)	VOC (L)	PCQM (L)	COCO (L)	Pf (L)	Ps (L)
	Accuracy $\uparrow$	Accuracy $\uparrow$	Accuracy $\uparrow$	Accuracy $\uparrow$	Accuracy $\uparrow$	F1 score $\uparrow$	MRR $\uparrow$	F1 score $\uparrow$	AP $\uparrow$	MAE $\downarrow$
Transformer	93.54 $\pm$ 0.43	89.78 $\pm$ 0.68	83.23 $\pm$ 0.75	50.69 $\pm$ 1.17	57.55 $\pm$ 0.53	26.94 $\pm$ 0.98	31.74 $\pm$ 0.20	<b>26.18<math>\pm</math>0.31</b>	63.26 $\pm$ 1.26	25.29 $\pm$ 0.16
w/ WaveGC	<b>94.77<math>\pm</math>0.30</b>	<b>93.93<math>\pm</math>0.62</b>	<b>89.69<math>\pm</math>0.66</b>	<b>63.97<math>\pm</math>1.49</b>	<b>71.69<math>\pm</math>0.26</b>	<b>29.42<math>\pm</math>0.94</b>	<b>33.30<math>\pm</math>0.10</b>	25.11 $\pm$ 0.25	<b>65.18<math>\pm</math>0.77</b>	<b>25.04<math>\pm</math>0.26</b>
SAN	93.82 $\pm$ 0.41	94.92 $\pm$ 0.38	91.31 $\pm$ 0.33	64.15 $\pm$ 1.01	70.25 $\pm$ 0.26	32.30 $\pm$ 0.39	33.50 $\pm$ 0.03	25.92 $\pm$ 1.58	63.84 $\pm$ 1.21	26.83 $\pm$ 0.43
w/ WaveGC	<b>95.47<math>\pm</math>0.31</b>	<b>95.51<math>\pm</math>0.22</b>	<b>91.64<math>\pm</math>0.42</b>	<b>66.65<math>\pm</math>0.83</b>	<b>71.98<math>\pm</math>0.23</b>	<b>33.33<math>\pm</math>0.91</b>	<b>34.23<math>\pm</math>0.13</b>	<b>26.06<math>\pm</math>0.78</b>	<b>64.54<math>\pm</math>0.37</b>	<b>26.06<math>\pm</math>0.17</b>
GraphGPS	95.47 $\pm$ 0.31	94.47 $\pm$ 0.46	89.51 $\pm$ 0.74	62.79 $\pm$ 0.72	71.45 $\pm$ 0.40	37.48 $\pm$ 1.09	33.37 $\pm$ 0.06	34.12 $\pm$ 0.44	65.35 $\pm$ 0.41	25.00 $\pm$ 0.05
w/ WaveGC	<b>95.89<math>\pm</math>0.34</b>	<b>95.37<math>\pm</math>0.44</b>	<b>91.00<math>\pm</math>0.48</b>	<b>69.14<math>\pm</math>0.78</b>	<b>72.85<math>\pm</math>0.24</b>	<b>40.24<math>\pm</math>0.28</b>	<b>34.50<math>\pm</math>0.02</b>	<b>35.01<math>\pm</math>0.22</b>	<b>70.10<math>\pm</math>0.27</b>	<b>24.95<math>\pm</math>0.07</b>

Table 3: Qualified results on short-range tasks compared to baselines. **Best**: Best, Underline: Runner-up, OOM: Out-of-memory, ‘\*’ Taken from original paper.

Model	CS	Photo	Computer	CoraFull	ogbn-arxiv
	Accuracy $\uparrow$	Accuracy $\uparrow$	Accuracy $\uparrow$	Accuracy $\uparrow$	Accuracy $\uparrow$
GCN [31]	92.92 $\pm$ 0.12	92.70 $\pm$ 0.20	89.65 $\pm$ 0.52	61.76 $\pm$ 0.14	71.74 $\pm$ 0.29
GAT [55]	93.61 $\pm$ 0.14	93.87 $\pm$ 0.11	90.78 $\pm$ 0.13	64.47 $\pm$ 0.18	71.82 $\pm$ 0.23
APPNP [16]	94.49 $\pm$ 0.07	94.32 $\pm$ 0.14	90.18 $\pm$ 0.17	65.16 $\pm$ 0.28	71.90 $\pm$ 0.25
GPRGNN [8]	95.13 $\pm$ 0.09	94.49 $\pm$ 0.14	89.32 $\pm$ 0.29	67.12 $\pm$ 0.31	71.78 $\pm$ 0.18
ChebNetII [21]	95.39 $\pm$ 0.39	94.71 $\pm$ 0.25	89.85 $\pm$ 0.85	<b>72.18<math>\pm</math>0.58</b>	72.32 $\pm$ 0.23
JacobiConv [56]	95.28 $\pm$ 0.32	95.43 $\pm$ 0.23*	90.39 $\pm$ 0.29*	70.02 $\pm$ 0.60	72.14 $\pm$ 0.17
OptBasisGNN [19]	88.33 $\pm$ 1.01	93.12 $\pm$ 0.43	89.65 $\pm$ 0.25	65.86 $\pm$ 1.03	72.27 $\pm$ 0.15*
Graphormer [64]	OOM	92.74 $\pm$ 0.14	OOM	OOM	OOM
Nodeformer [57]	95.28 $\pm$ 0.28	95.27 $\pm$ 0.22	91.12 $\pm$ 0.43	61.82 $\pm$ 0.81	59.90 $\pm$ 0.42
Specformer [3]	93.43 $\pm$ 0.35	95.48 $\pm$ 0.32*	<b>92.19<math>\pm</math>0.48</b>	68.41 $\pm$ 0.65	72.37 $\pm$ 0.18*
SGFormer [59]	93.63 $\pm$ 0.36	94.08 $\pm$ 0.35	91.17 $\pm$ 0.38	69.66 $\pm$ 0.63	<u>72.63<math>\pm</math>0.13</u> *
NAGphormer [7]	95.75 $\pm$ 0.09*	95.49 $\pm$ 0.11*	91.22 $\pm$ 0.14*	71.51 $\pm$ 0.13*	71.79 $\pm$ 0.37
Expformer [50]	95.77 $\pm$ 0.15*	95.27 $\pm$ 0.42*	91.59 $\pm$ 0.31*	65.42 $\pm$ 0.75	72.44 $\pm$ 0.28*
<b>WaveGC (ours)</b>	<b>95.89<math>\pm</math>0.34</b>	<b>95.51<math>\pm</math>0.22</b>	<u>91.64<math>\pm</math>0.42</u>	69.14 $\pm$ 0.78	<b>72.85<math>\pm</math>0.24</b>

Table 4: Qualified results on long-range tasks compared to baselines. **Best**: Best, Underline: Runner-up, OOM: Out-of-memory, ‘†’ Original code run by us.

Model	VOC	PCQM	COCO	Pf	Ps
	F1 score $\uparrow$	MRR $\uparrow$	F1 score $\uparrow$	AP $\uparrow$	MAE $\downarrow$
GCN [31]	12.68 $\pm$ 0.60	32.34 $\pm$ 0.06	08.41 $\pm$ 0.10	59.30 $\pm$ 0.23	34.96 $\pm$ 0.13
GINE [62]	12.65 $\pm$ 0.76	31.80 $\pm$ 0.27	13.39 $\pm$ 0.44	54.98 $\pm$ 0.79	35.47 $\pm$ 0.45
GatedGCN [4]	28.73 $\pm$ 2.19	32.18 $\pm$ 0.11	26.41 $\pm$ 0.45	58.64 $\pm$ 0.77	34.20 $\pm$ 0.13
ChebNetII <sup>†</sup> [21]	36.45 $\pm$ 0.52	34.34 $\pm$ 0.10	26.02 $\pm$ 0.53	68.19 $\pm$ 0.27	26.18 $\pm$ 0.58
JacobiConv <sup>†</sup> [56]	32.52 $\pm$ 0.87	34.24 $\pm$ 0.24	30.46 $\pm$ 0.46	68.00 $\pm$ 0.53	25.20 $\pm$ 0.21
OptBasisGNN <sup>†</sup> [19]	33.83 $\pm$ 0.61	32.42 $\pm$ 0.45	22.02 $\pm$ 0.18	61.92 $\pm$ 0.75	25.61 $\pm$ 0.19
GraphViT [22]	30.46 $\pm$ 1.15 <sup>†</sup>	32.80 $\pm$ 0.05 <sup>†</sup>	27.29 $\pm$ 0.49 <sup>†</sup>	69.42 $\pm$ 0.75	<b>24.49<math>\pm</math>0.16</b>
GRIT [41]	OOM <sup>†</sup>	34.33 $\pm$ 0.26 <sup>†</sup>	OOM <sup>†</sup>	<u>69.88<math>\pm</math>0.82</u>	<u>24.60<math>\pm</math>0.12</u>
Specformer [3] <sup>†</sup>	35.64 $\pm$ 0.85	33.73 $\pm$ 0.27	25.40 $\pm$ 0.55	66.86 $\pm$ 0.64	25.50 $\pm$ 0.14
Expformer [50]	39.60 $\pm$ 0.27	<b>36.37<math>\pm</math>0.20</b>	34.30 $\pm$ 0.08	65.27 $\pm$ 0.43	24.81 $\pm$ 0.07
<b>WaveGC (ours)</b>	<b>40.24<math>\pm</math>0.28</b>	<u>34.50<math>\pm</math>0.02</u>	<b>35.01<math>\pm</math>0.22</b>	<b>70.10<math>\pm</math>0.27</b>	24.95 $\pm$ 0.07

## 6.2 The effectiveness of matrix-valued kernel

Newly proposed matrix-valued kernel and weight-sharing technique constitutes the first advancement over graph convolution. In this section, we deeply explore the effectiveness of these two designs.

Observing the results from Table 5, the better performance from matrix-valued kernel indicates that more parameters on parameterizing kernels lead to enhanced feature learning. Meanwhile, upon analysis of Table 6, specifically learning kernels for each frequency does not yield improvement, and may even degrade performance. This degradation may be attributed to the large number of involved parameters, with potentially over-fitting. Matrix-valued kernels necessitates a mapping from each eigenvalue embedding to a specific matrix,  $f : \mathbb{R}^d \rightarrow \mathbb{R}^{d \times d}$ , which involves a MLP with



Table 5: Comparison between *Matrix-valued* and *Vector-valued* kernels.

Kernel	Photo (Accuracy $\uparrow$ )	Ps (MAE $\downarrow$ )
<i>Vector-valued</i>	94.61	25.30
<i>Matrix-valued</i>	<b>95.37</b>	<b>24.95</b>

Table 6: Comparison between *sharing* and *non-sharing* kernel weights

Result (Parameters)	CoraFull (Accuracy $\uparrow$ )	Ps (MAE $\downarrow$ )
<i>Non-sharing</i>	67.67 (883,215)	26.22 (1,410,029)
<i>Sharing</i>	<b>69.14 (621,135)</b>	<b>24.95 (534,701)</b>

weight dimension  $\mathbb{R}^{d \times d \times d}$ ,  $d$  is the embedding dimension. This results in a significant increase in the number of learnable parameters, as seen with  $d = 96$  in Ps, where the total number is nearly  $96 \times 96 \times 96 = 884,736$ .

### 6.3 The effectiveness of general wavelet bases

In this section, we compare the learnt wavelet bases from WaveGC with other baselines, including three graph wavelets and four polynomial bases as in Table 7. Here, ChebNet\* is a variant of our WaveGC where the only change is to combine odd and even terms without decomposition. Therefore, the improvement of WaveGC over ChebNet\* reflects the effectiveness of decoupling operation. The numerical comparison on Computer and PascalVOC-SP is shown in Table. 7, which demonstrates obvious gains from WaveGC especially on long-range PascalVOC-SP.

Table 7: Numerical comparison between WaveGC and other graph wavelets and polynomial bases

Model	Graph wavelet			Polynomial bases				Ours
	SGWT [20]	DEFT [2]	GWNN [61]	ChebNet*	ChebNetII [21]	JacobiConv [61]	OptBasisGNN [19]	WaveGC
Computer (Accuracy $\uparrow$ )	89.05	91.34	90.36	90.28	89.85	90.39	89.65	<b>91.64</b>
VOC (F1 score $\uparrow$ )	31.22	35.98	25.60	37.80	36.45	32.52	33.83	<b>40.24</b>

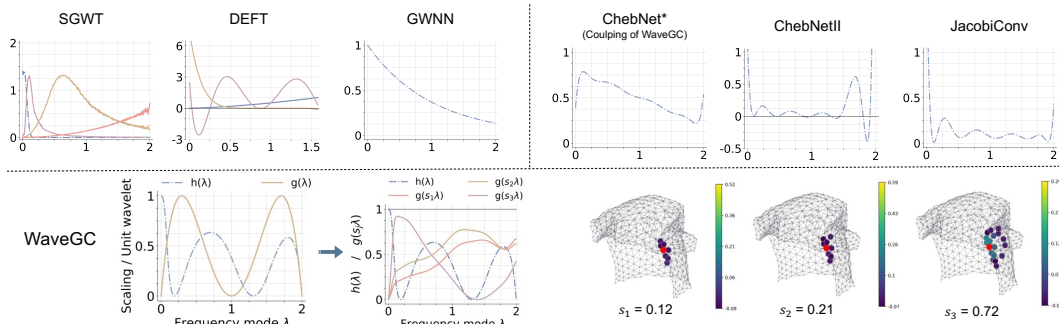


Figure 2: The spectral and spatial visualization of different bases on PascalVOC-SP.

To address the performance gap observed on the VOC dataset, we provide insights through the spectral visualization of various bases in Fig. 2<sup>1</sup>. These visualizations again confirm the disadvantages of other bases analyzed in section 5. For our WaveGC, the figure intuitively demonstrates that the unit wavelet got by decomposition of Chebyshev polynomials strictly meets the admissibility criteria, as Eq. (1), while the corresponding base scaling function supplements the direct current signals at  $\lambda = 0$ . We also depicts the signal distribution over the topology centered on the target node (the red-filled circle). The receptive field of the central node expands with the increasing of scale  $s$ , aggregating both short- and long-range information simultaneously. More analyses are given in Appendix D.3.

**Other experiments** In Appendix D.4, we analyze the effect of different components, and explore the mixing benefit between different architectures WaveGC, GCN and Transformer. Moreover, we also test our WaveGC on heterophily scenarios in Appendix D.5. Though WaveGC does not initially target on this topic, its positive performances convince us its potential to be further explored. In the end, we test the sensitivity of two important hyper-parameters in Appendix D.6.

<sup>1</sup>We do not visualize OptBasisGNN, as it learns bases with implicit recurring relation.

## 7 Conclusion

In this study, we proposed a novel graph convolution operation based on wavelets (WaveGC), establishing its theoretical capability to capture information at both short and long ranges through a multi-resolution approach.

**Limitation.** One potential limitation of WaveGC is the computational complexity. The main contribution of WaveGC is to address long-range interactions in graph convolution, so it inevitably establishes connections between most of nodes. This results in the same  $O(N^2)$  complexity as Transformer [54] and Specformer [3]. A possible solution is to decrease the number of considered frequency modes from  $N$  to  $\nu$ . In this way, the complexity is reduced to  $O(\nu \cdot N)$ . This operation makes WaveGC run on large-scale graph, i.e. ogbn-arxiv, and the best performance supports this simplification. Future work will focus on further simplification and scaling up to larger graphs.

## Acknowledgments and Disclosure of Funding

XB is supported by NUS Grant ID R-252-000-B97-133.

## References

- [1] G. Arfken. Convolution theorem. In *Mathematical Methods for Physicists*. Academic Press, 1985.
- [2] Anson Bastos, Abhishek Nadgeri, Kuldeep Singh, Toyotaro Suzumura, and Manish Singh. Learnable spectral wavelets on dynamic graphs to capture global interactions. In *Proceedings of the AAAI Conference on Artificial Intelligence*, volume 37, pages 6779–6787, 2023.
- [3] Deyu Bo, Chuan Shi, Lele Wang, and Renjie Liao. Specformer: Spectral graph neural networks meet transformers. In *The Eleventh International Conference on Learning Representations, ICLR 2023, Kigali, Rwanda, May 1-5, 2023*, 2023.
- [4] Xavier Bresson and Thomas Laurent. Residual gated graph convnets. *arXiv preprint arXiv:1711.07553*, 2017.
- [5] Joan Bruna, Wojciech Zaremba, Arthur Szlam, and Yann LeCun. Spectral networks and locally connected networks on graphs. *arXiv preprint arXiv:1312.6203*, 2013.
- [6] Dexiong Chen, Leslie O’Bray, and Karsten Borgwardt. Structure-aware transformer for graph representation learning. In *International Conference on Machine Learning*, pages 3469–3489. PMLR, 2022.
- [7] Jinsong Chen, Kaiyuan Gao, Gaichao Li, and Kun He. Nagphormer: A tokenized graph transformer for node classification in large graphs. In *The Eleventh International Conference on Learning Representations*, 2022.
- [8] Eli Chien, Jianhao Peng, Pan Li, and Olgica Milenkovic. Adaptive universal generalized pagerank graph neural network. *arXiv preprint arXiv:2006.07988*, 2020.
- [9] Hyuna Cho, Minjae Jeong, Sooyeon Jeon, Sungsoo Ahn, and Won Hwa Kim. Multi-resolution spectral coherence for graph generation with score-based diffusion. In *Thirty-seventh Conference on Neural Information Processing Systems*, 2023.
- [10] Fan RK Chung. *Spectral graph theory*, volume 92. American Mathematical Soc., 1997.
- [11] Michaël Defferrard, Xavier Bresson, and Pierre Vandergheynst. Convolutional neural networks on graphs with fast localized spectral filtering. *Advances in neural information processing systems*, 29, 2016.
- [12] Francesco Di Giovanni, T Konstantin Rusch, Michael M Bronstein, Andreea Deac, Marc Lackenby, Siddhartha Mishra, and Petar Veličković. How does over-squashing affect the power of gnns? *arXiv preprint arXiv:2306.03589*, 2023.

- [13] Vijay Prakash Dwivedi and Xavier Bresson. A generalization of transformer networks to graphs. *arXiv preprint arXiv:2012.09699*, 2020.
- [14] Vijay Prakash Dwivedi, Ladislav Rampásek, Michael Galkin, Ali Parviz, Guy Wolf, Anh Tuan Luu, and Dominique Beaini. Long range graph benchmark. *Advances in Neural Information Processing Systems*, 35:22326–22340, 2022.
- [15] Matthias Fey and Jan E. Lenssen. Fast graph representation learning with PyTorch Geometric. In *ICLR Workshop on Representation Learning on Graphs and Manifolds*, 2019.
- [16] Johannes Gasteiger, Aleksandar Bojchevski, and Stephan Günnemann. Predict then propagate: Graph neural networks meet personalized pagerank. *arXiv preprint arXiv:1810.05997*, 2018.
- [17] Simon Geisler, Yujia Li, Daniel J Mankowitz, Ali Taylan Cemgil, Stephan Günnemann, and Cosmin Paduraru. Transformers meet directed graphs. In *International Conference on Machine Learning*, pages 11144–11172. PMLR, 2023.
- [18] John Guibas, Morteza Mardani, Zongyi Li, Andrew Tao, Anima Anandkumar, and Bryan Catanzaro. Adaptive fourier neural operators: Efficient token mixers for transformers. *arXiv preprint arXiv:2111.13587*, 2021.
- [19] Yuhe Guo and Zhewei Wei. Graph neural networks with learnable and optimal polynomial bases. In *International Conference on Machine Learning*, pages 12077–12097. PMLR, 2023.
- [20] David K Hammond, Pierre Vandergheynst, and Rémi Gribonval. Wavelets on graphs via spectral graph theory. *Applied and Computational Harmonic Analysis*, 30(2):129–150, 2011.
- [21] Mingguo He, Zhewei Wei, and Ji-Rong Wen. Convolutional neural networks on graphs with chebyshev approximation, revisited. *Advances in neural information processing systems*, 35: 7264–7276, 2022.
- [22] Xiaoxin He, Bryan Hooi, Thomas Laurent, Adam Perold, Yann LeCun, and Xavier Bresson. A generalization of vit/mlp-mixer to graphs. In *International Conference on Machine Learning*, pages 12724–12745. PMLR, 2023.
- [23] Geoffrey Hinton, Li Deng, Dong Yu, George E Dahl, Abdel-rahman Mohamed, Navdeep Jaitly, Andrew Senior, Vincent Vanhoucke, Patrick Nguyen, Tara N Sainath, et al. Deep neural networks for acoustic modeling in speech recognition: The shared views of four research groups. *IEEE Signal processing magazine*, 29(6):82–97, 2012.
- [24] Lars Hörmander. Fourier integral operators. i. 1971.
- [25] Weihua Hu, Matthias Fey, Marinka Zitnik, Yuxiao Dong, Hongyu Ren, Bowen Liu, Michele Catasta, and Jure Leskovec. Open graph benchmark: Datasets for machine learning on graphs. *Advances in neural information processing systems*, 33:22118–22133, 2020.
- [26] Weihua Hu, Matthias Fey, Hongyu Ren, Maho Nakata, Yuxiao Dong, and Jure Leskovec. Ogb-lsc: A large-scale challenge for machine learning on graphs. *arXiv preprint arXiv:2103.09430*, 2021.
- [27] Md. Shamim Hussain, Mohammed J. Zaki, and Dharmashankar Subramanian. Global self-attention as a replacement for graph convolution. In *KDD '22: The 28th ACM SIGKDD Conference on Knowledge Discovery and Data Mining, Washington, DC, USA, August 14 - 18, 2022*, pages 655–665. ACM, 2022.
- [28] Truong Son Hy and Risi Kondor. Multiresolution matrix factorization and wavelet networks on graphs. In *Topological, Algebraic and Geometric Learning Workshops 2022*, pages 172–182. PMLR, 2022.
- [29] Bowen Jin, Yu Zhang, Yu Meng, and Jiawei Han. Edgeformers: Graph-empowered transformers for representation learning on textual-edge networks. In *The Eleventh International Conference on Learning Representations, ICLR 2023, Kigali, Rwanda, May 1-5, 2023*, 2023.

- [30] Xuan Kan, Wei Dai, Hejie Cui, Zilong Zhang, Ying Guo, and Carl J. Yang. Brain network transformer. In *Advances in Neural Information Processing Systems 35: Annual Conference on Neural Information Processing Systems 2022, NeurIPS 2022, New Orleans, LA, USA, November 28 - December 9, 2022*, 2022.
- [31] Thomas N. Kipf and Max Welling. Semi-supervised classification with graph convolutional networks. In *5th International Conference on Learning Representations, ICLR 2017, Toulon, France, April 24-26, 2017, Conference Track Proceedings*, 2017.
- [32] Devin Kreuzer, Dominique Beaini, Will Hamilton, Vincent Létourneau, and Prudencio Tossou. Rethinking graph transformers with spectral attention. *Advances in Neural Information Processing Systems*, 34:21618–21629, 2021.
- [33] Alex Krizhevsky, Ilya Sutskever, and Geoffrey E Hinton. Imagenet classification with deep convolutional neural networks. *Advances in neural information processing systems*, 25, 2012.
- [34] Brian Kulis, Kate Saenko, and Trevor Darrell. What you saw is not what you get: Domain adaptation using asymmetric kernel transforms. In *CVPR 2011*, pages 1785–1792. IEEE, 2011.
- [35] Yann LeCun, Léon Bottou, Yoshua Bengio, and Patrick Haffner. Gradient-based learning applied to document recognition. *Proceedings of the IEEE*, 86(11):2278–2324, 1998.
- [36] Nora Leonardi and Dimitri Van De Ville. Tight wavelet frames on multislice graphs. *IEEE Transactions on Signal Processing*, 61(13):3357–3367, 2013.
- [37] Ron Levie, Federico Monti, Xavier Bresson, and Michael M Bronstein. Cayleynets: Graph convolutional neural networks with complex rational spectral filters. *IEEE Transactions on Signal Processing*, 67(1):97–109, 2018.
- [38] Qimai Li, Zhichao Han, and Xiao-Ming Wu. Deeper insights into graph convolutional networks for semi-supervised learning. In *Proceedings of the AAAI conference on artificial intelligence*, volume 32, 2018.
- [39] Zongyi Li, Nikola Borislavov Kovachki, Kamyar Aizzadenesheli, Burigede Liu, Kaushik Bhattacharya, Andrew M. Stuart, and Anima Anandkumar. Fourier neural operator for parametric partial differential equations. In *9th International Conference on Learning Representations, ICLR 2021, Virtual Event, Austria, May 3-7, 2021*, 2021.
- [40] László Lovász. Random walks on graphs. *Combinatorics, Paul erdos is eighty*, 2(1-46):4, 1993.
- [41] Liheng Ma, Chen Lin, Derek Lim, Adriana Romero-Soriano, Puneet K. Dokania, Mark Coates, Philip H. S. Torr, and Ser-Nam Lim. Graph inductive biases in transformers without message passing. In *International Conference on Machine Learning, ICML 2023, 23-29 July 2023, Honolulu, Hawaii, USA*, volume 202, pages 23321–23337. PMLR, 2023.
- [42] Stéphane Mallat. *A Wavelet Tour of Signal Processing, 2nd Edition*. Academic Press, 1999.
- [43] Grégoire Mialon, Dexiong Chen, Margot Selsosse, and Julien Mairal. Graphit: Encoding graph structure in transformers. *arXiv preprint arXiv:2106.05667*, 2021.
- [44] Alan V Oppenheim, Alan S Willsky, Syed Hamid Nawab, and Jian-Jiun Ding. *Signals and systems*, volume 2. Prentice hall Upper Saddle River, NJ, 1997.
- [45] Hongbin Pei, Bingzhe Wei, Kevin Chen-Chuan Chang, Yu Lei, and Bo Yang. Geom-gcn: Geometric graph convolutional networks. *arXiv preprint arXiv:2002.05287*, 2020.
- [46] Oleg Platonov, Denis Kuznedelev, Michael Diskin, Artem Babenko, and Liudmila Prokhorenkova. A critical look at the evaluation of gnns under heterophily: Are we really making progress? *arXiv preprint arXiv:2302.11640*, 2023.
- [47] Ladislav Rampásek, Michael Galkin, Vijay Prakash Dwivedi, Anh Tuan Luu, Guy Wolf, and Dominique Beaini. Recipe for a general, powerful, scalable graph transformer. In *Advances in Neural Information Processing Systems 35: Annual Conference on Neural Information Processing Systems 2022, NeurIPS 2022, New Orleans, LA, USA, November 28 - December 9, 2022*, 2022.

- [48] Yu Rong, Yatao Bian, Tingyang Xu, Weiyang Xie, Ying Wei, Wenbing Huang, and Junzhou Huang. Self-supervised graph transformer on large-scale molecular data. In *Advances in Neural Information Processing Systems 33: Annual Conference on Neural Information Processing Systems 2020, NeurIPS 2020, December 6-12, 2020, virtual*, 2020.
- [49] Yangmei Shen, Wenrui Dai, Chenglin Li, Junni Zou, and Hongkai Xiong. Multi-scale graph convolutional network with spectral graph wavelet frame. *IEEE Transactions on Signal and Information Processing over Networks*, 7:595–610, 2021.
- [50] Hamed Shirzad, Ameya Velingker, Balaji Venkatachalam, Danica J. Sutherland, and Ali Kemal Sinop. Exphormer: Sparse transformers for graphs. In *International Conference on Machine Learning, ICML 2023, 23-29 July 2023, Honolulu, Hawaii, USA*, volume 202, pages 31613–31632. PMLR, 2023.
- [51] David I Shuman, Sunil K Narang, Pascal Frossard, Antonio Ortega, and Pierre Vandergheynst. The emerging field of signal processing on graphs: Extending high-dimensional data analysis to networks and other irregular domains. *IEEE signal processing magazine*, 30(3):83–98, 2013.
- [52] David I Shuman, Christoph Wiesmeyer, Nicki Holighaus, and Pierre Vandergheynst. Spectrum-adapted tight graph wavelet and vertex-frequency frames. *IEEE Transactions on Signal Processing*, 63(16):4223–4235, 2015.
- [53] Yao-Hung Hubert Tsai, Shaojie Bai, Makoto Yamada, Louis-Philippe Morency, and Ruslan Salakhutdinov. Transformer dissection: a unified understanding of transformer’s attention via the lens of kernel. *arXiv preprint arXiv:1908.11775*, 2019.
- [54] Ashish Vaswani, Noam Shazeer, Niki Parmar, Jakob Uszkoreit, Llion Jones, Aidan N Gomez, Łukasz Kaiser, and Illia Polosukhin. Attention is all you need. *Advances in neural information processing systems*, 30, 2017.
- [55] Petar Velickovic, Guillem Cucurull, Arantxa Casanova, Adriana Romero, Pietro Lio, Yoshua Bengio, et al. Graph attention networks. *stat*, 1050(20):10–48550, 2017.
- [56] Xiyuan Wang and Muhan Zhang. How powerful are spectral graph neural networks. In *International Conference on Machine Learning*, pages 23341–23362. PMLR, 2022.
- [57] Qitian Wu, Wentao Zhao, Zenan Li, David P Wipf, and Junchi Yan. Nodeformer: A scalable graph structure learning transformer for node classification. *Advances in Neural Information Processing Systems*, 35:27387–27401, 2022.
- [58] Qitian Wu, Chenxiao Yang, Wentao Zhao, Yixuan He, David Wipf, and Junchi Yan. Diffformer: Scalable (graph) transformers induced by energy constrained diffusion. In *The Eleventh International Conference on Learning Representations, ICLR 2023, Kigali, Rwanda, May 1-5, 2023*, 2023.
- [59] Qitian Wu, Wentao Zhao, Chenxiao Yang, Hengrui Zhang, Fan Nie, Haitian Jiang, Yatao Bian, and Junchi Yan. Simplifying and empowering transformers for large-graph representations. *arXiv preprint arXiv:2306.10759*, 2023.
- [60] Zhanghao Wu, Paras Jain, Matthew Wright, Azalia Mirhoseini, Joseph E Gonzalez, and Ion Stoica. Representing long-range context for graph neural networks with global attention. *Advances in Neural Information Processing Systems*, 34:13266–13279, 2021.
- [61] Bingbing Xu, Huawei Shen, Qi Cao, Yunqi Qiu, and Xueqi Cheng. Graph wavelet neural network. In *7th International Conference on Learning Representations, ICLR 2019, New Orleans, LA, USA, May 6-9, 2019*, 2019.
- [62] Keyulu Xu, Weihua Hu, Jure Leskovec, and Stefanie Jegelka. How powerful are graph neural networks? In *7th International Conference on Learning Representations, ICLR 2019, New Orleans, LA, USA, May 6-9, 2019*, 2019.
- [63] Mingxing Xu, Wenrui Dai, Chenglin Li, Junni Zou, Hongkai Xiong, and Pascal Frossard. Graph neural networks with lifting-based adaptive graph wavelets. *IEEE Transactions on Signal and Information Processing over Networks*, 8:63–77, 2022.

- [64] Chengxuan Ying, Tianle Cai, Shengjie Luo, Shuxin Zheng, Guolin Ke, Di He, Yanming Shen, and Tie-Yan Liu. Do transformers really perform badly for graph representation? *Advances in Neural Information Processing Systems*, 34:28877–28888, 2021.
- [65] Zaixi Zhang, Qi Liu, Qingyong Hu, and Chee-Kong Lee. Hierarchical graph transformer with adaptive node sampling. *Advances in Neural Information Processing Systems*, 35:21171–21183, 2022.
- [66] Xuebin Zheng, Bingxin Zhou, Junbin Gao, Yuguang Wang, Pietro Lió, Ming Li, and Guido Montúfar. How framelets enhance graph neural networks. In *Proceedings of the 38th International Conference on Machine Learning, ICML 2021, 18-24 July 2021, Virtual Event*, volume 139, pages 12761–12771, 2021.

## A Theoretical Proof

Firstly, we give two auxiliary but indispensable lemma and theorem. Let starts from the formula  $\sigma(\Psi_s \mathbf{H}^{(l)} \mathbf{W}_s^{(l)})$ . In this equation, we bound the first derivate of non-linear function as  $|\sigma'| < c_\sigma$ , and set  $\|\mathbf{W}_s^{(l)}\| \leq w$ , where  $\|\cdot\|$  is the operator norm. First, we give an upper bound for each entry in  $\Psi_s$ .

**Lemma A.1 (Upper bound for graph wavelet).** *Let  $\Psi = \mathbf{U}g(\Lambda)\mathbf{U}^T$ . Given a large even number  $K > 0$ , suppose  $g$  is  $K + 1$  times continuously differentiable on  $[0, 2]$  and satisfies  $g(0) = 0, g^{(r)}(0) = 0$  for all  $r < K$ , and  $g^{(K)}(0) = C > 0$ . Then, for  $\forall i, j \in V \times V$ , we have:*

$$(\Psi_s)_{ij} < \left( \alpha (\hat{\mathbf{A}})^{K/2} s^K \right)_{ij}, \quad \alpha = \frac{C \cdot 2^K (K + 1)}{K!}. \quad (18)$$

The proof is given in Appendix A.1. In this lemma, we assume  $g$  is smooth enough at  $\lambda = 0$ . For fair comparison with traditional one-hop message passing framework  $\sigma(\mathbf{A}\mathbf{H}^{(l)}\mathbf{W}_s^{(l)})$ , we just test the flexibility with the similar form  $\sigma(\Psi_s \mathbf{H}^{(l)} \mathbf{W}_s^{(l)})$ . In this case, we derive the depth  $m_\Psi$  necessary for this wavelet basis  $\Psi_s$  to induce the amount of mixing  $\text{mix}_{y_G}(a, b)$  between two nodes  $a$  and  $b$ .

**Theorem A.2 (The least depth for mixing).** *Given commute time  $\tau(a, b)$  [40] and number of edges  $|E|$ . If  $\Psi_s$  generates mixing  $\text{mix}_{y_G}(b, a)$ , then the number of layers  $m_\Psi$  satisfies*

$$m_\Psi \geq \frac{\tau(a, b)}{2K} + \frac{2|E|}{K\sqrt{d_a d_b}} \left[ \frac{\text{mix}_{y_G}(b, a)}{\gamma(\alpha^2 s^{2K})^{m_\Psi}} - \frac{1}{\lambda_1} (\gamma + |1 - \lambda^*|^{K m_\Psi + 1}) \right], \quad (19)$$

where  $d_a$  and  $d_b$  are degrees of two nodes,  $\gamma = \sqrt{\frac{d_{\max}}{d_{\min}}}$ , and  $|1 - \lambda^*| = \max_{0 < n \leq N-1} |1 - \lambda_n| < 1$ .

The proof is given in Appendix A.2. In the following subsections, we firstly prove these lemma and theorem, and finally give the complete proof of Theorem 4.3.

### A.1 Proof of Lemma A.1 (Upper bound for graph wavelet)

*Proof.* We aim to investigate the properties of filters  $\Psi_{s_j} = \mathbf{U}g(s_j \lambda)\mathbf{U}^T$  to capture both global and local information, corresponding to the cases  $s_j \rightarrow 0$  and  $s_j \rightarrow \infty$ , respectively. In the former case, as  $s_j$  approaches zero,  $g(s_j \lambda)$  tends towards  $g(0)$ . For the latter case, the spectral information becomes densely distributed and concentrated near zero. Hence, the meaningful analysis of  $g(\lambda)$  primarily revolves around  $\lambda = 0$ . Expanding  $g(\lambda)$  using Taylor's series around  $\lambda = 0$ , we get:

$$g(\lambda) = C \frac{\lambda^K}{K!} + g^{(K+1)}(\lambda^*) \frac{\lambda^{K+1}}{(K+1)!} \approx C \frac{\lambda^K}{K!}, \quad (20)$$

where we neglect the high-order remainder term. Next, we have

$$\begin{aligned} (\Psi)_{ij} &= (\mathbf{U}g(\Lambda)\mathbf{U}^T)_{ij} = \left( C \frac{\hat{\mathbf{L}}^K}{K!} \right)_{ij} \\ &= \left( \frac{C}{K!} (\mathbf{I} - \hat{\mathbf{A}})^K \right)_{ij} = \left( \frac{C}{K!} \sum_{p=0}^K \binom{K}{p} (-\hat{\mathbf{A}})^p \right)_{ij} \\ &< \left( \frac{C}{K!} \sum_{p=0}^K \binom{K}{p} (\hat{\mathbf{A}})^p \right)_{ij} = \left( \frac{C}{K!} \sum_{p=0}^K \frac{K!}{(K-p)!p!} (\hat{\mathbf{A}})^p \right)_{ij} \\ &= \left( C \sum_{p=0}^K \frac{(\hat{\mathbf{A}})^p}{(K-p)!p!} \right)_{ij}. \end{aligned} \quad (21a)$$

Let us explore the expression  $\epsilon_{ij}^p = \frac{(\hat{\mathbf{A}})_{ij}^p}{(K-p)!p!}$ . First, we will address the denominator  $(K-p)!p!$ . As  $p$  increases, this denominator experiences a sharp decrease followed by a rapid increase. The

minimum value occurs at  $(K/2)!(K/2)!$  when  $p = K/2$ , assuming  $K$  is even. Second, let's analyze the numerator  $(\hat{\mathbf{A}})_{ij}^p$ , which involves repeated multiplication of  $\hat{\mathbf{A}}$ . According to Theorem 1 in [38], this repeated multiplication causes  $(\hat{\mathbf{A}})^p$  to converge to the eigenspaces spanned by the eigenvector  $D^{-1/2}\mathbf{1}$  of  $\lambda = 0$ , where  $\mathbf{1} = (1, 1, \dots, 1) \in \mathbb{R}^n$ . Then, let us assume there exists a value  $p^*$  beyond which the change in  $(\hat{\mathbf{A}})^p$  becomes negligible. Given that  $K$  is a large even number, we can infer that  $K/2 \gg p^*$ . Thus, when  $(K-p)!p!$  sharply decreases,  $(\hat{\mathbf{A}})^p$  has already approached a stationary state. Consequently,  $\max \epsilon_{ij}^p = \frac{(\hat{\mathbf{A}})_{ij}^{K/2}}{(K/2)!(K/2)!}$ , where the denominator reaches its minimum.

Thus, we have

$$\begin{aligned} (\Psi)_{ij} &< \left( C \sum_{p=0}^K \frac{(\hat{\mathbf{A}})^p}{(K-p)!p!} \right)_{ij} \\ &< C(K+1) \left( \frac{(\hat{\mathbf{A}})^{K/2}}{(K/2)!(K/2)!} \right)_{ij} \\ &< \left( \frac{C \cdot 2^K (K+1)}{K!} (\hat{\mathbf{A}})^{K/2} \right)_{ij}. \end{aligned} \quad (22a)$$

We have  $\frac{1}{(K/2)!(K/2)!} < \frac{2^K}{K!}$  given that

$$\begin{aligned} (K/2)!(K/2)! &= \left( \frac{K}{2} \cdot \frac{K-2}{2} \cdots \frac{4}{2} \cdot \frac{2}{2} \right) \left( \frac{K}{2} \cdot \frac{K-2}{2} \cdots \frac{4}{2} \cdot \frac{2}{2} \right) \\ &> \left( \frac{K}{2} \cdot \frac{K-2}{2} \cdots \frac{4}{2} \cdot \frac{2}{2} \right) \left( \frac{K-1}{2} \cdot \frac{K-3}{2} \cdots \frac{3}{2} \cdot \frac{1}{2} \right) \\ &= \underbrace{K \cdot K-1 \cdot K-2 \cdot K-3 \cdots 4 \cdot 3 \cdot 2 \cdot 1}_{K \text{ terms}} = \frac{K!}{2^K}. \end{aligned} \quad (23)$$

With  $\alpha = \frac{C \cdot 2^K (K+1)}{K!}$  and scale  $s$ , Eq. (22a) can be finally written as

$$(\Psi_s)_{ij} < \left( \alpha (\hat{\mathbf{A}})^{K/2} s^K \right)_{ij}. \quad (24)$$

□

## A.2 Proof of Theorem A.2 (The least depth for mixing)

For this section, we mainly refer to the proof from [12].

**Preliminary.** For simplicity, we follow [12] to denote some operations utilized in this section. As stated, we consider the message passing formula  $\sigma(\Psi_s \mathbf{H}^{(l)} \mathbf{W}_s^{(l)})$ . First, we denote  $\mathbf{h}_a^{(l),\alpha}$  as the  $\alpha$ -th entry of the embedding  $\mathbf{h}_a^{(l)}$  for node  $a$  at the  $l$ -th layer. Then, we rewrite the formula as:

$$\mathbf{h}_a^{(l),\alpha} = \sigma(\tilde{\mathbf{h}}_a^{(l-1),\alpha}), \quad 1 \leq \alpha \leq d, \quad (25)$$

where  $\tilde{\mathbf{h}}_a^{(l-1),\alpha} = (\Psi_s \mathbf{H}^{(l)} \mathbf{W}_s^{(l)})_a$  is the entry  $\alpha$  of the pre-activated embedding of node  $a$  at layer  $l$ . Given nodes  $a$  and  $b$ , we denote the following differentiation operations:

$$\nabla_a \mathbf{h}_b^{(l)} := \frac{\partial \mathbf{h}_b^{(l)}}{\partial \mathbf{x}_a}, \quad \nabla_{ab}^2 \mathbf{h}_i^{(l)} := \frac{\partial^2 \mathbf{h}_i^{(l)}}{\partial \mathbf{x}_a \partial \mathbf{x}_b}. \quad (26)$$

Next, we firstly derive upper bounds on  $\nabla_a \mathbf{h}_b^{(l)}$ , and then on  $\nabla_{ab}^2 \mathbf{h}_i^{(l)}$ .

<sup>2</sup>Simple proof.  $(\hat{\mathbf{A}})^p = \mathbf{U}(\mathbf{I} - \mathbf{\Lambda})^p \mathbf{U}^\top = \sum_{i=0}^p \binom{p}{i} (-1)^i \lambda_i \mathbf{u}_1 \mathbf{u}_1^\top$ . Provided only  $1 - \lambda_0 = 1$  and  $1 - \lambda_i \in (-1, 1)$  for other eigenvalues, with  $p \rightarrow \infty$ , only  $(1 - \lambda_0)^p = 1$  but  $(1 - \lambda_i)^p \rightarrow 0$ . Thus, we have  $(\hat{\mathbf{A}})^p \rightarrow \mathbf{u}_1 \mathbf{u}_1^\top$ , where  $\mathbf{u}_1 = D^{-1/2} \mathbf{1}$ .



**Lemma A.3.** Given the message passing formula  $\sigma(\Psi_s \mathbf{H}^{(l)} \mathbf{W}_s^{(l)})$ , let assume  $|\sigma'| \leq c_\sigma$  and  $\|\mathbf{W}^{(l)}\| \leq w$ , where  $\|\cdot\|$  is the operator norm. For two nodes  $a$  and  $b$  after  $l$  layers of message passing, the following holds:

$$\|\nabla_a \mathbf{h}_b^{(l)}\| \leq (c_\sigma w)^l (\mathbf{B}^l)_{ba}, \quad (27)$$

where  $\mathbf{B}_{ba} = \left(\alpha(\hat{\mathbf{A}})^{K/2} s^K\right)_{ba}$ .

*Proof.* If  $l = 1$  and we fix entries  $1 \leq \alpha, \beta \leq d$ , then we have:

$$(\nabla_a \mathbf{h}_b^{(1)})_{\alpha\beta} = (\text{diag}(\sigma'(\tilde{\mathbf{h}}_b^{(0)}))(\mathbf{W}^{(1)} \Psi_{ba} \mathbf{I}))_{\alpha\beta}. \quad (28)$$

With Cauchy–Schwarz inequality, we bound the left hand side by

$$\begin{aligned} \|\nabla_a \mathbf{h}_b^{(1)}\| &\leq \|\text{diag}(\sigma'(\tilde{\mathbf{h}}_b^{(0)}))\| \cdot \|\mathbf{W}^{(1)} \Psi_{ba}\| \\ &\leq c_\sigma w \mathbf{B}_{ba}. \end{aligned}$$

Next, we turn to a general case where  $l > 1$ :

$$(\nabla_a \mathbf{h}_b^{(l)})_{\alpha\beta} = (\text{diag}(\sigma'(\tilde{\mathbf{h}}_b^{(l-1)}))(\mathbf{W}^{(l)} \sum_j \Psi_{bj} \nabla_a \mathbf{h}_j^{(m-1)}))_{\alpha\beta}. \quad (30)$$

Then, we can use the induction step to bound the above equation:

$$\begin{aligned} \|\nabla_a \mathbf{h}_b^{(l)}\| &\leq (c_\sigma w)^l \left| \sum_{j_0} \sum_{j_1} \cdots \sum_{j_{l-2}} \Psi_{bj_0} \Psi_{j_0 j_1} \cdots \Psi_{j_{l-3} j_{l-2}} \Psi_{j_{l-2} a} \right| \\ &\leq (c_\sigma w)^l (\mathbf{B}^l)_{ba}. \end{aligned} \quad (31)$$

In Eq. (31), we implicitly use  $|\Psi_s^l|_{ba} < \left(\alpha(\hat{\mathbf{A}})^{K/2} s^K\right)_{ba}^l = \mathbf{B}_{ba}^l$ . Similar to proof given in Appendix A.1, we can give the following proof:

$$\begin{aligned} |\Psi_s^l|_{ba} &= |\mathbf{U} g(s\Lambda)^l \mathbf{U}^T|_{ba} = \left| s^{lK} C^l \frac{\hat{\mathcal{L}}^{lK}}{K!^l} \right|_{ba} \\ &= \left| s^{lK} \frac{C^l}{K!^l} (\mathbf{I} - \hat{\mathbf{A}})^{lK} \right|_{ba} = \left| s^{lK} \frac{C^l}{K!^l} \sum_{p=0}^{lK} \binom{lK}{p} (-\hat{\mathbf{A}})^p \right|_{ba} \\ &< \left( s^{lK} \frac{C^l}{K!^l} \sum_{p=0}^{lK} \binom{lK}{p} (\hat{\mathbf{A}})^p \right)_{ba} = \left( s^{lK} \frac{C^l}{K!^l} \sum_{p=0}^{lK} \frac{(lK)!}{(lK-p)!p!} (\hat{\mathbf{A}})^p \right)_{ba} \\ &= \left( s^{lK} \frac{C^l (lK)!}{K!^l} \sum_{p=0}^{lK} \frac{(\hat{\mathbf{A}})^p}{(lK-p)!p!} \right)_{ba} < \left( s^{lK} \frac{C^l (lK)!}{K!^l} (lK+1) \left( \frac{(\hat{\mathbf{A}})^{lK/2}}{(lK/2)!(lK/2)!} \right) \right)_{ba} \\ &< \left( s^{lK} \frac{C^l (lK)!}{K!^l} (lK+1) \frac{2^{lK}}{(lK)!} (\hat{\mathbf{A}})^{lK/2} \right)_{ba} = \left( s^{lK} \frac{C^l \cdot 2^{lK} (lK+1)}{K!^l} (\hat{\mathbf{A}})^{lK/2} \right)_{ba} \\ &< \left( s^{lK} \frac{C^l \cdot 2^{lK} (K+1)^l}{K!^l} (\hat{\mathbf{A}})^{lK/2} \right)_{ba} = \left( \alpha(\hat{\mathbf{A}})^{K/2} s^K \right)_{ba}^l, \end{aligned} \quad (32)$$

where in the last line, we utilize the relation  $lK+1 < (K+1)^l$ .  $\square$

**Lemma A.4.** Given the message passing formula  $\sigma(\Psi_s \mathbf{H}^{(l)} \mathbf{W}_s^{(l)})$ , let assume  $|\sigma'|, |\sigma''| \leq c_\sigma$  and  $\|\mathbf{W}^{(l)}\| \leq w$ , where  $\|\cdot\|$  is operator norm. For nodes  $i, a$  and  $b$  after  $l$  layers of message passing, the following holds:

$$\|\nabla_{ab}^2 \mathbf{h}_i^{(l)}\| \leq \sum_{k=0}^{l-1} \sum_{j \in \mathcal{V}} (c_\sigma w)^{2l-k-1} w (\mathbf{B}^{l-k})_{jb} (\mathbf{B}^k)_{ij} (\mathbf{B}^{l-k})_{ja}, \quad (33)$$

where  $\mathbf{B}_{ba} = \left(\alpha(\hat{\mathbf{A}})^{K/2} s^K\right)_{ba}$ .

*Proof.* Considering  $\nabla_{ab}^2 \mathbf{h}_i^{(l)} \in \mathbb{R}^{d \times (d \times d)}$ , we refer to [12] to use the following ordering for indexing the columns:

$$\frac{\partial^2 \mathbf{h}_i^{(l), \alpha}}{\partial x_b^\beta \partial x_a^\gamma} := (\nabla_{ab}^2 \mathbf{h}_i^{(l)})_{\alpha, d(\beta-1)+\gamma}. \quad (34)$$

Similar to the proof of Lemma A.3, we firstly focus on  $m = 1$ :

$$(\nabla_{ab}^2 \mathbf{h}_i^{(1)})_{\alpha, d(\beta-1)+\gamma} = (\text{diag}(\sigma''(\tilde{\mathbf{h}}_i^{(0), \alpha}))(\mathbf{W}^{(1)} \Psi_{ib} \mathbf{I})_{\alpha\gamma} \times (\mathbf{W}^{(1)} \Psi_{ia} \mathbf{I})_{\alpha\beta}). \quad (35)$$

We bound the left-hand side as:

$$\|\nabla_{ab}^2 \mathbf{h}_i^{(1)}\| \leq (c_\sigma w)(w|\mathbf{B}_{ib}||\mathbf{B}_{ia}|). \quad (36)$$

Then, for  $m > 1$ :

$$\begin{aligned} & (\nabla_{ab}^2 \mathbf{h}_i^{(l)})_{\alpha, d(\beta-1)+\gamma} \\ &= \underbrace{\text{diag}(\sigma''(\tilde{\mathbf{h}}_i^{(l-1), \alpha}))(\mathbf{W}^{(l)} \sum_j \Psi_{ij} \nabla_a \mathbf{h}_j^{(l-1)}) \times (\mathbf{W}^{(l)} \sum_j \Psi_{ij} \nabla_b \mathbf{h}_j^{(l-1)})}_{\mathbf{R}} \\ &+ \underbrace{\text{diag}(\sigma'(\tilde{\mathbf{h}}_i^{(l-1), \alpha}))(\mathbf{W}^{(m)} \sum_j \Psi_{ij} \nabla_{ab}^2 \mathbf{h}_j^{(l-1)})}_{\mathbf{Z}}. \end{aligned} \quad (37)$$

We denote  $\|\nabla_j \mathbf{h}_i^{(l-1)}\|$  as  $(D\mathbf{h}^{(l-1)})_{ij}$ , and  $\|\nabla_{ab}^2 \mathbf{h}_i^{(l-1)}\|$  as  $(D^2 \mathbf{h}^{(l-1)})_{ba}i$ . To bound  $\mathbf{R}$ , we deduce as follows:

$$\begin{aligned} \|\mathbf{R}\| &\leq c_\sigma w \sum_j \mathbf{B}_{ij} \|\nabla_a \mathbf{h}_j^{(l-1)}\| \times (w \sum_j \mathbf{B}_{ij} \|\nabla_b \mathbf{h}_j^{(l-1)}\|) \\ &= c_\sigma w (w \mathbf{B} D \mathbf{h}^{(l-1)})_{ib} (\mathbf{B} D \mathbf{h}^{(l-1)})_{ia} \\ &\leq c_\sigma w (w \mathbf{B} (c_\sigma w)^{l-1} \mathbf{B}^{l-1})_{ib} (\mathbf{B} (c_\sigma w)^{l-1} \mathbf{B}^{l-1})_{ia} \\ &= (c_\sigma w)^{2l-1} (w (\mathbf{B}^l)_{ib} (\mathbf{B}^l)_{ia}), \end{aligned} \quad (38a)$$

where we utilize the conclusion from Theorem A.3 in (38a). For term  $\mathbf{Z}$ , we have:

$$\begin{aligned} \|\mathbf{Z}\| &\leq c_\sigma w (\mathbf{B} D^2 \mathbf{h}^{(l-1)})_i \\ &\leq c_\sigma w \sum_s \mathbf{B}_{is} \sum_{k=0}^{l-2} \sum_{j \in V} (c_\sigma w)^{2l-2-k-1} w (\mathbf{B}^{l-1-k})_{jb} (\mathbf{B}^k)_{sj} (\mathbf{B}^{l-1-k})_{ja} \\ &= \sum_{k=0}^{l-2} \sum_{j \in V} (c_\sigma w)^{2l-2-k} (\mathbf{B}^{l-1-k})_{jb} (\mathbf{B}^{k+1})_{ij} (\mathbf{B}^{l-1-k})_{ja} \\ &= \sum_{k=1}^{l-1} \sum_{j \in V} (c_\sigma w)^{2l-1-k} (\mathbf{B}^{l-k})_{jb} (\mathbf{B}^k)_{ij} (\mathbf{B}^{l-k})_{ja}, \end{aligned} \quad (39a)$$

where in (39a), we recursively use the Eq. (37). Finally, we finish the proof as:

$$\begin{aligned} \|\nabla_{ab}^2 \mathbf{h}_i^{(l)}\| &\leq \|\mathbf{R}\| + \|\mathbf{Z}\| \\ &\leq \sum_{k=0}^{l-1} \sum_{j \in V} (c_\sigma w)^{2l-1-k} (\mathbf{B}^{l-k})_{jb} (\mathbf{B}^k)_{ij} (\mathbf{B}^{l-k})_{ja}. \end{aligned} \quad (40)$$

□

With Lemma A.3 and A.4, now we give the following theorem.

**Theorem A.5.** Consider the message passing formula  $\sigma(\Psi_s \mathbf{H}^{(l)} \mathbf{W}_s^{(l)})$  with  $m_\Psi$  layers, the induced mixing  $\text{mix}_{y_G}(b, a)$  over the features of nodes  $a$  and  $b$  satisfies:

$$\text{mix}_{y_G}(b, a) \leq \sum_{l=0}^{m_\Psi-1} (c_\sigma w)^{(2m_\Psi-l-1)} \left( w (\mathbf{B}^{m_\Psi-l})^\top \text{diag}(\mathbf{1}^\top \mathbf{B}^l) \mathbf{B}^{m_\Psi-l} \right)_{ab}, \quad (41)$$

where  $\mathbf{B}_{ba} = \left( \alpha (\hat{\mathbf{A}})^{K/2} s^K \right)_{ba}$  and  $\mathbf{1} \in \mathbb{R}^n$  is the vector of ones.

*Proof.* Here, we define the prediction function  $y_G : N \times d \rightarrow d$  on  $G$  as  $y_G^{(m_\Psi)} = \text{Readout}(\mathbf{H}^{(m_\Psi)}\boldsymbol{\theta})$ , where  $\text{Readout}$  is to gather all nodes embeddings to get the final graph embedding,  $\mathbf{H}^{(m_\Psi)}$  is the node embedding matrix after  $m_\Psi$  layers and  $\boldsymbol{\theta}$  is the learnable weight for graph-level task. If we set  $\text{Readout} = \text{sum}$ , we derive:

$$\begin{aligned} \text{mix}_{y_G}(b, a) &= \max_x \max_{1 \leq \beta, \gamma \leq d} \left| \frac{\partial^2 y_G^{(m_\Psi)}(\mathbf{X})}{\partial \mathbf{x}_a^\beta \partial \mathbf{x}_b^\gamma} \right| \\ &\leq \sum_{i \in V} \left| \sum_{\alpha=1}^d \theta_\alpha \frac{\partial^2 h_i^{(m_\Psi), \alpha}}{\partial \mathbf{x}_a^\beta \partial \mathbf{x}_b^\gamma} \right| \\ &= \sum_{i \in V} \|(\nabla_{ab}^2 \mathbf{h}_i^{(m_\Psi)})^\top \boldsymbol{\theta}\| \\ &\leq \sum_{i \in V} \|\nabla_{ab}^2 \mathbf{h}_i^{(m_\Psi)}\| \end{aligned} \quad (42a)$$

$$\leq \sum_{k=0}^{m_\Psi-1} (c_\sigma w)^{(2m_\Psi-k-1)} \left( w (\mathbf{B}^{m_\Psi-k})^\top \text{diag}(\mathbf{1}^\top \mathbf{B}^k) \mathbf{B}^{m_\Psi-k} \right)_{ab}, \quad (42b)$$

□

where in (42a), we assume the norm  $\|\boldsymbol{\theta}\| \leq 1$ . In (42b), we use the results from Lemma A.4. This upper bound still holds if  $\text{Readout}$  is chosen as  $\text{MEAN}$  or  $\text{MAX}$  [12].

In theorem A.5, we can assume that  $c_\sigma$  to be smaller or equal than one, which is satisfied by the majority of current active functions. Furthermore, considering the normalization (e.g.,  $L_2$  norm) on  $\mathbf{W}^{(l)}$ , we assume  $w < 1$ . With these two assumptions, the conclusion of theorem A.5 is rewritten as:

$$\text{mix}_{y_G}(b, a) \leq \sum_{l=0}^{m_\Psi-1} \left( (\mathbf{B}^{m_\Psi-l})^\top \text{diag}(\mathbf{1}^\top \mathbf{B}^l) \mathbf{B}^{m_\Psi-l} \right)_{ab}. \quad (43)$$

With this new conclusion, we now turn to the proof of Theorem A.2:

*Proof.* Firstly,  $\text{diag}(\mathbf{1}^\top \mathbf{B}^l)_i = (\alpha s^K)^l ((\hat{\mathbf{A}})^{K/2})^l \mathbf{1}_i \leq \gamma (\alpha s^K)^l$  by using  $((\hat{\mathbf{A}})^{K/2})^l \mathbf{1}_i \leq \gamma$  [12]. Then, we find

$$\begin{aligned} \sum_{l=0}^{m_\Psi-1} \left( (\mathbf{B}^{m_\Psi-l})^\top \text{diag}(\mathbf{1}^\top \mathbf{B}^l) \mathbf{B}^{m_\Psi-l} \right)_{ab} &\leq \gamma \left( \sum_{l=0}^{m_\Psi-1} \mathbf{B}^{2(m_\Psi-l)} \cdot (\alpha s^K)^l \right)_{ab} \\ &< \gamma \left( \sum_{l=0}^{m_\Psi-1} (\alpha (\hat{\mathbf{A}})^{K/2} s^K)^{2(m_\Psi-l)} \cdot (\alpha s^K)^l \right)_{ab} \\ &< \gamma (\alpha s^K)^{2m_\Psi} \left( \sum_{l=0}^{m_\Psi-1} \hat{\mathbf{A}}^{K(m_\Psi-l)} \right)_{ab} \\ &= \gamma (\alpha s^K)^{2m_\Psi} \left( \sum_{l=1}^{m_\Psi} \hat{\mathbf{A}}^{Kl} \right)_{ab}. \end{aligned} \quad (44)$$

The following proof depends on *commute time*  $\tau(a, b)$  [40], whose the definition is as follows using the spectral representation of the graph Laplacian [12]:

$$\tau(a, b) = 2|E| \sum_{n=0}^{N-1} \frac{1}{\lambda_n} \left( \frac{u_n(a)}{\sqrt{d_a}} - \frac{u_n(b)}{\sqrt{d_b}} \right)^2. \quad (45)$$

Then, we have:

$$\begin{aligned}
\left( \sum_{l=1}^{m_\Psi} \hat{A}^{Kl} \right)_{ab} &\leq \sum_{l=0}^{Km_\Psi} (\hat{A}^l)_{ab} \\
&= \sum_{l=0}^{Km_\Psi} \sum_{n \geq 0} (1 - \lambda_n)^l u_n(a) u_n(b) \\
&= (Km_\Psi + 1) \frac{\sqrt{d_a d_b}}{2|E|} + \sum_{n>0} \frac{1 - (1 - \lambda)^{Km_\Psi + 1}}{\lambda_n} u_n(a) u_n(b) \\
&= (Km_\Psi + 1) \frac{\sqrt{d_a d_b}}{2|E|} + \sum_{n>0} \frac{1}{\lambda_n} u_n(a) u_n(b) - \sum_{n>0} \frac{(1 - \lambda)^{Km_\Psi + 1}}{\lambda_n} u_n(a) u_n(b).
\end{aligned} \tag{46a}$$

In Eq. (46a), we use  $u_0(a) = \sqrt{\frac{d_a}{2|E|}}$ . Then, from the definition of commute time, we can get:

$$\begin{aligned}
\sum_{n=1}^{N-1} \frac{1}{\lambda_n} u_n(a) u_n(b) &= \frac{-\tau(a, b)}{4|E|} \sqrt{d_a d_b} + \frac{1}{2} \sum_{n>0} \frac{1}{\lambda_n} (u_n^2(a) \sqrt{\frac{d_b}{d_a}} + u_n^2(b) \sqrt{\frac{d_a}{d_b}}) \\
&\leq \frac{-\tau(a, b)}{4|E|} \sqrt{d_a d_b} + \frac{1}{2\lambda_1} \left( \sqrt{\frac{d_a}{d_b}} + \sqrt{\frac{d_b}{d_a}} - \frac{\sqrt{d_a d_b}}{|E|} \right),
\end{aligned} \tag{47}$$

where in the last inequation, we utilize the fact that  $\sum_{n>0} u_n^2(a) = 1 - u_0^2(a)$  because  $\{u_n\}$  is a set of orthonormal basis. Besides, we use  $\lambda_n > \lambda_1, \forall n > 1$ . Next, we derive

$$\begin{aligned}
-\sum_{n>0} \frac{(1 - \lambda)^{Km_\Psi + 1}}{\lambda_n} u_n(a) u_n(b) &\leq \sum_{n>0} \frac{|1 - \lambda^*|^{Km_\Psi + 1}}{\lambda_n} |u_n(a) u_n(b)| \\
&\leq \frac{|1 - \lambda^*|^{Km_\Psi + 1}}{2\lambda_1} \sum_{n>0} (u_n^2(a) + u_n^2(b)) \\
&\leq \frac{|1 - \lambda^*|^{Km_\Psi + 1}}{2\lambda_1} \left( 2 - \frac{d_a + d_b}{2|E|} \right),
\end{aligned} \tag{48}$$

where  $|1 - \lambda^*| = \max_{0 < n \leq N-1} |1 - \lambda_n| < 1$ . Insert derivations (47) and (48) into (46), then gather all above derivations:

$$\begin{aligned}
\text{mix}_{y_G}(b, a) &\leq \gamma(\alpha s^K)^{2m_\Psi} \left\{ (Km_\Psi + 1) \frac{\sqrt{d_a d_b}}{2|E|} - \frac{\tau(a, b)}{4|E|} \sqrt{d_a d_b} \right. \\
&\quad \left. + \frac{1}{2\lambda_1} \left( \sqrt{\frac{d_a}{d_b}} + \sqrt{\frac{d_b}{d_a}} - \frac{\sqrt{d_a d_b}}{|E|} \right) + \frac{|1 - \lambda^*|^{Km_\Psi + 1}}{2\lambda_1} \left( 2 - \frac{d_a + d_b}{2|E|} \right) \right\} \\
&\leq \gamma(\alpha s^K)^{2m_\Psi} \sqrt{d_a d_b} \left( \frac{Km_\Psi}{2|E|} - \frac{\tau(a, b)}{4|E|} \right) + \frac{\gamma(\alpha s^K)^{2m_\Psi}}{2\lambda_1} \left( \sqrt{\frac{d_a}{d_b}} + \sqrt{\frac{d_b}{d_a}} \right) + \frac{\gamma(\alpha s^K)^{2m_\Psi}}{\lambda_1} |1 - \lambda^*|^{Km_\Psi + 1}.
\end{aligned} \tag{49}$$

In last inequation, we discard  $\frac{\sqrt{d_a d_b}}{2|E|} \left[ 1 - \frac{1}{\lambda_1} \left( 1 + \frac{|1 - \lambda^*|^{Km_\Psi + 1}}{2} \left( \sqrt{\frac{d_a}{d_b}} + \sqrt{\frac{d_b}{d_a}} \right) \right) \right] < 0$  because  $\lambda_1 < 1$ . Then,

$$\frac{\text{mix}_{y_G}(b, a)}{\gamma(\alpha s^K)^{2m_\Psi} \sqrt{d_a d_b}} \leq \frac{Km_\Psi}{2|E|} - \frac{\tau(a, b)}{4|E|} + \frac{1}{2\lambda_1 \sqrt{d_a d_b}} \left( \sqrt{\frac{d_a}{d_b}} + \sqrt{\frac{d_b}{d_a}} + 2|1 - \lambda^*|^{Km_\Psi + 1} \right). \tag{50}$$

From (50), we can finally give the lower bound of  $m_\Psi$  as:

$$\begin{aligned}
m_\Psi &\geq \frac{2|E|}{K} \left\{ \frac{\tau(a,b)}{4|E|} + \frac{\text{mix}_{y_G}(b,a)}{\gamma(\alpha s^K)^{2m_\Psi} \sqrt{d_a d_b}} - \frac{1}{2\lambda_1 \sqrt{d_a d_b}} \left( \sqrt{\frac{d_a}{d_b}} + \sqrt{\frac{d_b}{d_a}} + 2|1 - \lambda^*|^{Km_\Psi+1} \right) \right\} \\
&> \frac{2|E|}{K} \left\{ \frac{\tau(a,b)}{4|E|} + \frac{1}{\sqrt{d_a d_b}} \left[ \frac{\text{mix}_{y_G}(b,a)}{\gamma(\alpha s^K)^{2m_\Psi}} - \frac{1}{2\lambda_1} (2\gamma + 2|1 - \lambda^*|^{Km_\Psi+1}) \right] \right\} \\
&= \frac{2|E|}{K} \left\{ \frac{\tau(a,b)}{4|E|} + \frac{1}{\sqrt{d_a d_b}} \left[ \frac{\text{mix}_{y_G}(b,a)}{\gamma(\alpha^2 s^{2K})^{m_\Psi}} - \frac{1}{\lambda_1} (\gamma + |1 - \lambda^*|^{Km_\Psi+1}) \right] \right\} \\
&= \frac{\tau(a,b)}{2K} + \frac{2|E|}{K\sqrt{d_a d_b}} \left[ \frac{\text{mix}_{y_G}(b,a)}{\gamma(\alpha^2 s^{2K})^{m_\Psi}} - \frac{1}{\lambda_1} (\gamma + |1 - \lambda^*|^{Km_\Psi+1}) \right]
\end{aligned} \tag{51}$$

### A.3 Proof of Theorem 4.3 (Short-range and long-range receptive fields)

*Proof.* From theorem A.2, we denote  $L_{m_\Psi} = \frac{\tau(a,b)}{2K} + \frac{2|E|}{K\sqrt{d_a d_b}} \left[ \frac{\text{mix}_{y_G}(b,a)}{\gamma(\alpha^2 s^{2K})^{m_\Psi}} - \frac{1}{\lambda_1} (\gamma + |1 - \lambda^*|^{Km_\Psi+1}) \right]$ . Similar to the proof A.2, if we consider the one-hop message passing  $\sigma(\mathbf{A}\mathbf{H}^{(l)}\mathbf{W}_s^{(l)})$ , an analogous lower bound is obtained:

$$L_{m_A} = \frac{\tau(a,b)}{4} + \frac{|E|}{\sqrt{d_a d_b}} \left[ \frac{\text{mix}_{y_G}(b,a)}{\gamma} - \frac{1}{\lambda_1} (\gamma + |1 - \lambda^*|^{2m_A+1}) \right]. \tag{52}$$

Therefore, we have

$$L_{m_\Psi} \approx \frac{2}{K} L_{m_A} + \frac{2|E|}{K\sqrt{d_a d_b}} \left[ \frac{\text{mix}_{y_G}(b,a)}{\gamma} \left( \frac{1}{(\alpha^2 s^{2K})^{m_\Psi}} - 1 \right) \right], \tag{53}$$

where we ignore  $|1 - \lambda^*|^{Km_\Psi+1}$  and  $|1 - \lambda^*|^{2m_A+1}$ . Since  $|1 - \lambda^*| < 1$  as shown in theorem A.2, therefore  $|1 - \lambda^*|^{Km_\Psi+1} - |1 - \lambda^*|^{2m_A+1}$  will be very small, especially when  $m_\Psi$  and  $m_A$  are large. From Eq. (53), when  $s \rightarrow \infty$ , the relation becomes:

$$L_{m_\Psi} \approx \frac{2}{K} L_{m_A} - \frac{2|E|}{K\sqrt{d_a d_b}} \frac{\text{mix}_{y_G}(b,a)}{\gamma}. \tag{54}$$

Or, when  $s \rightarrow 0$ , the relation becomes:

$$L_{m_\Psi} \approx \frac{2}{K} L_{m_A} + \frac{2|E|}{K\sqrt{d_a d_b}} \frac{\text{mix}_{y_G}(b,a)}{\gamma} \cdot \frac{1}{(\alpha^2 s^{2K})^{m_\Psi}}. \tag{55}$$

□

## B Relationship between Graph Convolution and Transformer

To recap, the vanilla Transformer [54] is given as:

$$\mathbf{H}^{(l+1)} = \text{softmax} \left( \frac{\mathbf{H}^{(l)} \mathbf{W}_q (\mathbf{H}^{(l)} \mathbf{W}_k)^\top}{\sqrt{d}} \right) \mathbf{H}^{(l)} \mathbf{W}_v, \tag{56}$$

where  $\mathbf{H}^{(l)}, \mathbf{H}^{(l+1)} \in \mathbb{R}^{N \times d}$  are node embeddings from  $l$ th and  $(l+1)$ th layers, and  $\{\mathbf{W}_q, \mathbf{W}_k, \mathbf{W}_v\} \in \mathbb{R}^{d \times d}$  are the query, key, and value learnable matrices. This self-attention mechanism can be written as a kernel summation in the discrete case [43, 53, 18]. Specifically for node  $s$ ,  $\mathbf{h}_s^{(l+1)} = \sum_t \kappa(s, t) \mathbf{h}_t^{(l)}$ , where  $\kappa(s, t) = \text{softmax} \left( \frac{\mathbf{H}^{(l)} \mathbf{W}_q (\mathbf{H}^{(l)} \mathbf{W}_k)^\top}{\sqrt{d}} \right)_{(s,t)} \cdot \mathbf{W}_v$ . Therefore,

$\kappa : \{1, \dots, N\} \times \{1, \dots, N\} \rightarrow \mathbb{R}^{d \times d}$  is treated as an asymmetric matrix-valued kernel. Note that the usage of asymmetric kernel is also commonly used in various machine learning tasks [34]. Further assume  $\kappa(s, t) = \kappa(s - t)$ , which indicates a shift-invariant GT since the attention depends on the difference between two nodes rather than their positions. Then, Eq. (56) becomes a convolution  $\mathbf{h}_s^{(l+1)} = \sum_t \kappa(s - t) \mathbf{h}_t^{(l)}$ , which can be expressed with the convolution theorem as:

$$\mathbf{h}_s^{(l+1)} = \mathcal{F}^{-1}(\mathcal{F}(\kappa) \cdot \mathcal{F}(\mathbf{H}^{(l)}))(s) \in \mathbb{R}^{1 \times d}. \tag{57}$$

Eq. (57) is also known as Fourier integral operator [24]. In Eq. (57), for each frequency mode  $n \in N$  (i.e.,  $\mathcal{F}(\mathbf{H}^{(l)})(n, \cdot)$ ),  $\mathcal{F}(\boldsymbol{\kappa})(n) \in \mathbb{R}^{d \times d}$ , because  $\boldsymbol{\kappa} : \{1, \dots, N\} \times \{1, \dots, N\} \rightarrow \mathbb{R}^{d \times d}$ . Hence, for all modes,  $\mathcal{F}(\boldsymbol{\kappa})$  can be fully parameterized by a neural network  $R_\theta \in \mathbb{R}^{N \times d \times d}$  [39]:

$$\mathbf{h}_s^{(l+1)} = \mathcal{F}^{-1}(R_\theta \cdot \mathcal{F}(\mathbf{H}^{(l)}))(s) \in \mathbb{R}^{1 \times d}. \quad (58)$$

## C Details of Encoding Eigenvalues

In this paper, we adopt Eigenvalue Encoding (EE) Module [3] to encode eigenvalues. EE functions as a set-to-set spectral filter, enabling interactions between eigenvalues. In EE, both magnitudes and relative differences of all eigenvalues are leveraged. Specifically, the authors use an eigenvalue encoding function to transform each  $\lambda$  from scalar  $\mathbb{R}^1$  to a vector  $\mathbb{R}^d$ :

$$\rho(\lambda, 2i) = \sin(\epsilon\lambda/10000^{2i/d}), \quad \rho(\lambda, 2i+1) = \cos(\epsilon\lambda/10000^{2i/d}), \quad (59)$$

where  $i$  is the dimension of the representations and  $\epsilon$  is a hyper parameter. By encoding in this way, relative frequency shifts between eigenvalues are captured. Then, the raw representations of eigenvalues are the concatenation between eigenvalues and corresponding representation vectors:

$$\mathbf{Z}_\lambda = [\lambda_1 || \rho(\lambda_1), \dots, \lambda_N || \rho(\lambda_N)]^\top \in \mathbb{R}^{N \times (d+1)}. \quad (60)$$

To capture the dependencies between eigenvalues, a standard Transformer is used followed by skip-connection and feed forward network (FFN):

$$\hat{\mathbf{Z}}_\lambda = \text{Transformer}(\text{LN}(\mathbf{Z}_\lambda)) + \mathbf{Z}_\lambda \in \mathbb{R}^{N \times (d+1)}, \quad \mathbf{Z} = \text{FFN}(\text{LN}(\hat{\mathbf{Z}}_\lambda)) + \hat{\mathbf{Z}}_\lambda \in \mathbb{R}^{N \times (d+1)}, \quad (61)$$

where LN is the layer normalization. Then,  $\mathbf{Z}$  is the embedding matrix for eigenvalues, which is injected into the learning of combination coefficients  $\tilde{\mathbf{a}}$  and  $\tilde{\mathbf{b}}$ , and scales  $\tilde{\mathbf{s}}$ .

## D Experimental Details

### D.1 Implementation Details

For the short-range task, we present the results of all baselines from NAGphormer [7] and Ex-phormer [50], excluding three base models (Transformer, SAN, and GraphGPS). This omission is due to the necessity of knowing the parameters of these base models for parameter freezing, while such information is unavailable. Consequently, we provide the results of these three models based on our experiments. For the long-range task, we showcase the outcomes of GCN, GINE, GatedGCN, Transformer, SAN+LapPE, SAN+RWSE from [14], alongside the results of the remaining baselines sourced from their original papers.

Considering that our WaveGC replaces the Transformer in each base model, we focus on tuning the parameters newly introduced by WaveGC while keeping the others unchanged. Specifically, we explore the number of truncated terms  $\rho$  from 1 to 10 and adjust the number of scales  $J$  from 1 to 5. Additionally, for the pre-defined vector  $\bar{\mathbf{s}}$  controlling the amplitudes of scales, we test each element in  $\bar{\mathbf{s}}$  from 0.1 to 10. The usage of the tight frames constraint is also a parameter subject to tuning, contingent on the given dataset. Typically, models iterate through several layers to produce a single result, thus the parameters of WaveGC may or may not be shared between different layers. Finally, due to the large scale of short-range datasets, we implement two strategies to prevent out-of-memory issues. Firstly, only the first 30% of eigenvalues and their corresponding eigenvectors are retained for training in each dataset. Secondly, for the learned scaling function basis  $\Phi$  and multiple wavelet bases  $\Psi_{s_j}$ , we set a threshold  $\aleph$  and filter out entries in  $\Phi$  and  $\Psi_{s_j}$  whose absolute value is lower than  $\aleph$ .

For fair comparisons, we randomly run 4 times on long-range datasets [14], and 10 times on short-range datasets [7], and report the average results with their standard deviation for all methods. For the sake of reproducibility, we also report the related parameters in Appendix D.8.

### D.2 Datasets Description

For short-range datasets, we choose five commonly used CS, Photo, Computer, CoraFull [15] and ogbn-arxiv [25]. CS is a network based on co-authorship, with nodes representing authors

Table 8: The statistics of the short-range datasets.

Dataset	# Graphs	# Nodes	# Edges	# Features	# Classes
CS	1	18,333	163,788	6,805	15
Photo	1	7,650	238,163	745	8
Computer	1	13,752	491,722	767	10
CoraFull	1	19,793	126,842	8,710	70
ogbn-arxiv	1	169,343	1,116,243	128	40

and edges symbolizing collaboration between them. In the Photo and Computer networks, nodes stand for items, and edges suggest that the connected items are often purchased together, forming co-purchase networks. CoraFull is a network focused on citations, where nodes are papers and edges indicate citation connections between them. ogbn-arxiv is a citation network among all Computer Science (CS) Arxiv papers, where each node corresponds to an Arxiv paper, and the edges indicate the citations between papers. The details of these five datasets are summarized in Table 8.

Table 9: The statistics of the long-range datasets.

Dataset	# Graphs	Avg. # nodes	Avg. # edges	Prediction level	Task	Metric
PascalVOC-SP	11,355	479.4	2,710.5	inductive node	21-class classif.	F1 score
PCQM-Contact	529,434	30.1	61.0	inductive link	link ranking	MRR
COCO-SP	123,286	476.9	2,693.7	inductive node	81-class classif.	F1 score
Peptides-func	15,535	150.9	307.3	graph	10-task classif.	Avg. Precision
Peptides-struct	15,535	150.9	307.3	graph	11-task regression	Mean Abs. Error

For long-range tasks, we choose five long-range datasets [14], including PascalVOC-SP (VOC), PCQM-Contact (PCQM), COCO-SP (COCO), Peptides-func (Pf) and Peptides-struct (Ps). These five datasets are usually used to test the performance of different transformer architectures. VOC and COCO datasets are created through SLIC superpixelization of the Pascal VOC and MS COCO image collections. They are both utilized for node classification, where each super-pixel node is categorized into a specific object class. PCQM is developed from PCQM4Mv2 [26] and its related 3D molecular structures, focusing on binary link prediction. This involves identifying node pairs that are in 3D contact but distant in the 2D graph. Both Pf and Ps datasets consist of atomic graphs of peptides sourced from SATPdb. In the Peptides-func dataset, the task involves multi-label graph classification into 10 distinct peptide functional classes. Conversely, the Peptides-struct dataset is centered on graph regression to predict 11 different 3D structural properties of peptides. The details of these five datasets are summarized in Table 9.

### D.3 More analyses for section 6.3

In this section, we provide more analyses on the visualization performances for different bases. Upon examination of three kinds of wavelets (i.e., {SGWT, DEFT, GWNN}), those from SGWT meet admissibility criteria with multiple resolutions, but these cubic splines are not adaptive. DEFT outputs several bases with unpredictable shapes, so it is hard to strictly restrain these outputs as wavelets. GWNN adopts one exponential wavelet base, omitting information from different ranges as well as not meeting criteria. The following three polynomial bases (i.e., ChebNet\*, ChebNetII and JacobiConv) comprehensively entangles signals from different frequency intervals, where crucial band-pass signals for long-range tasks are overwhelmed. Consequentially, these bases blend local and distant information in spatial space, hampering the decision on the best range. For our WaveGC, Fig. 2 intuitively demonstrates that the unit wavelet got by our decoupling of Chebyshev polynomials strictly meets the admissibility criteria, as Eq. (1), while the corresponding base scaling function supplements the direct current signals at  $\lambda = 0$ . After integration of learnable scales, the final wavelets also meet criteria and adapt to the demand on multiresolution. The plot of  $G(\lambda) = h(\lambda)^2 + \sum_{j=1}^3 g(s_j \lambda)^2$  as a black dashed line (located at 1) confirms the construction of tight frames via normalization technique. Fig.2 also depicts the signal distribution over the topology centered on the target node (the red-filled circle). This figure also demonstrates that as the scale  $s_j$  increases, the receptive field of the central node expands. Once again, this visualization intuitively confirms the capability of WaveGC to aggregate both short- and long-range information simultaneously but distinguishingly.

To give one more example, we provide additional visualization results on the CoraFull dataset. These results are presented in Fig. 3, where the learned scaling functions  $h(\lambda)$  and  $g(\lambda)$  meet the specified requirements. The four subfigures in Fig. 3(c) illustrate that as the scale  $s_j$  increases, the receptive field of the center node expands. This highlights WaveGC’s capability to capture both short- and long-range information by adjusting different values of  $s_j$ . However, one of our strategies for CoraFull involves considering only 30% of eigenvalues as input. Consequently, the full spectrum is truncated, leaving only the remaining 30% parts, as depicted in Fig. 4. As shown in Fig. 4(b), all  $g(s_j\lambda)$  functions behave like band-pass filters with large  $s_j$  values due to this truncation. Consequently, all three learned wavelets enable the center node to receive distant information, as demonstrated in Fig. 4(c).

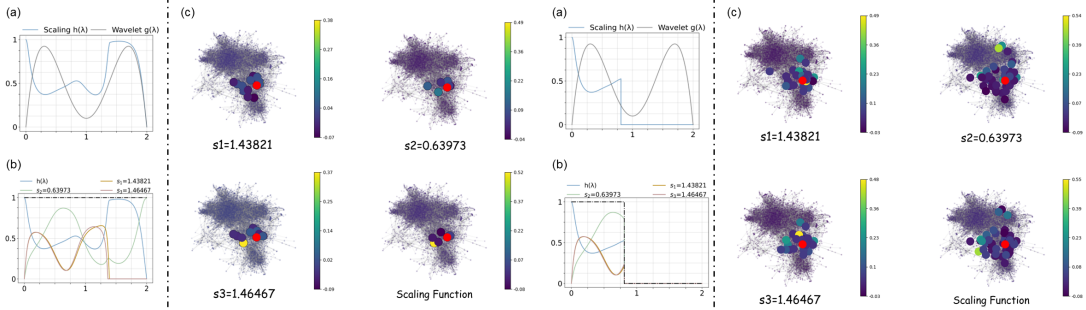


Figure 3: Illustration of the spectral and spatial signals of the learned function basis and multiple wavelet bases with full spectrum.

Figure 4: Illustration of the spectral and spatial signals of the learned function basis and multiple wavelet bases with partial spectrum.

#### D.4 More ablation study

Table 10: Results of the ablation study. **Bold:** Best.

Variants	Pf	VOC	Computer	CoraFull
	AP $\uparrow$	F1 score $\uparrow$	Accuracy $\uparrow$	Accuracy $\uparrow$
w/o $h(\lambda)$	56.56	15.69	89.37	63.36
w/o $g(s_j\lambda)$	61.89	25.51	89.67	63.78
w/o tight frame	64.71	27.79	<b>89.77</b>	<b>64.74</b>
<b>Ours</b>	<b>65.18</b>	<b>29.42</b>	89.69	63.97

Table 11: Different combinations between WaveGC GCN and Transformer. **Bold:** Best.

Combinations	Pf	Photo
	AP $\uparrow$	Accuracy $\uparrow$
MPGNN + Transformer	94.47	65.35
WaveGC + Transformer	95.04	67.57
WaveGC + MPGNN	<b>95.37</b>	<b>70.10</b>

In this section, we conduct an ablation study of our WaveGC to assess the effectiveness of each component, and the corresponding results are presented in Table 10. The table compares Transformer+WaveGC with several variants. These variants involve removing the scaling function basis (denoted as ‘w/o  $h(\lambda)$ ’), excluding multiple wavelet bases (denoted as w/o ‘ $g(s_j\lambda)$ ’), or eliminating the constraint on tight frames (denoted as ‘w/o tight frame’). The evaluation is conducted on two long-range datasets (Pf and VOC) and two short-range datasets (Computer and CoraFull). (1) Both the scaling function basis  $h(\lambda)$  and wavelet bases  $g(s_j\lambda)$  are essential components of our WaveGC. In particular, neglecting  $h(\lambda)$  results in a significant drop in performance, emphasizing the crucial role of low-frequency information. (2) The tight frame constraint proves beneficial for Pf and VOC datasets but is less effective for Computer and CoraFull. This suggests a trade-off, as the tight frame constraint limits the flexibility of the learned filters, and the impact depends on the given datasets.

This work involves three frameworks, including MPGNN (graph convolution), Transformer and WaveGC, and exploring the benefits of combination between these frameworks is also an interesting topic. The related results are given in Table 11. Upon comparing the first two combinations in the table, ‘Transformer’ primarily focuses on capturing global information, while ‘MPGNN’ or ‘WaveGC’ are expected to focus on local information. Given that MPGNN is proficient in depicting local structure, the improvement from WaveGC is somewhat limited. However, in the third combination ‘MPGNN+WaveGC’, WaveGC is designed to capture both local and global information.



The noticeable improvement compared to ‘MPGNN+Transformer’ can be attributed to the flexibility and multi-resolution capabilities of WaveGC. In summary, both MPGNN and WaveGC are effective at capturing local structure, while WaveGC excels in encoding long-range information. For practical applications, it is advisable to select the specific encoder based on the characteristics of the given graph.

### D.5 Experimental results on heterophily datasets

Besides the short-rang and long-range tasks, heterophily benchmark datasets are also important scenarios for testing graph spectral methods. Here, we choose three heterophily datasets, including Actor [45], Minesweeper and Tolokers [46]. Table 12 shows their basic statistics. We firstly compare WaveGC with corresponding base models (Table 13), and then compare with other graph Transformers (Table 14), including {Graphormer, Nodeformer, Specformer, SGFormer, NAGphormer and Exphormer}. Again, our WaveGC outperforms both base models and other powerful graph Transformers. Especially, for Minesweeper and Tolokers, WaveGC also defeats other baselines reported in the original paper [46]. This hints that aggregating information from different distance probably alleviate heterophily from neighbors to some extent.

Table 12: The statistics of the heterophily datasets.

Dataset	# Graphs	# Nodes	# Edges	# Features	# Classes
Actor	1	7,600	33,544	932	5
Minesweeper	1	10,000	39,402	7	2
Tolokers	1	11,758	519,000	10	2

Table 13: Quantified results (i.e.  $\% \pm \sigma$ ) on heterophily datasets compared to base models.

Model	Actor	Minesweeper	Tolokers
	Accuracy $\uparrow$	ROC AUC $\uparrow$	ROC AUC $\uparrow$
Transformer	37.63 $\pm$ 0.55	50.75 $\pm$ 1.14	74.04 $\pm$ 0.53
<b>Transformer+WaveGC</b>	<b>38.61<math>\pm</math>0.74</b>	<b>93.19<math>\pm</math>1.56</b>	<b>82.81<math>\pm</math>1.12</b>
SAN	31.18 $\pm$ 1.08	92.07 $\pm$ 0.35	<b>83.37<math>\pm</math>0.55</b>
<b>SAN+WaveGC</b>	<b>33.63<math>\pm</math>0.82</b>	<b>93.98<math>\pm</math>0.60</b>	82.73 $\pm$ 0.98
GraphGPS	36.52 $\pm$ 0.56	94.03 $\pm$ 0.42	84.63 $\pm$ 0.88
<b>GraphGPS+WaveGC</b>	<b>37.40<math>\pm</math>1.04</b>	<b>94.81<math>\pm</math>0.42</b>	<b>85.38<math>\pm</math>0.52</b>

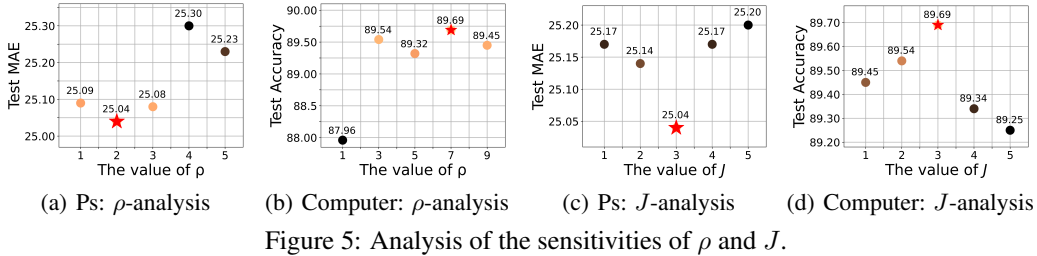
Table 14: Qualified results (i.e.  $\% \pm \sigma$ ) on heterophily tasks compared to baselines. **Bold:** Best, Underline: Runner-up, ‘\*’ Taken from original papers.

Model	Actor	Minesweeper	Tolokers
	Accuracy $\uparrow$	ROC AUC $\uparrow$	ROC AUC $\uparrow$
Graphormer	36.41 $\pm$ 0.49	90.89 $\pm$ 0.53	82.75 $\pm$ 0.88
Nodeformer	34.62 $\pm$ 0.82	86.71 $\pm$ 0.88	78.10 $\pm$ 1.03
Spcformer	<b>41.93<math>\pm</math>1.04*</b>	89.93 $\pm$ 0.41	80.42 $\pm$ 0.55
SGFormer	37.90 $\pm$ 1.10	<u>94.31<math>\pm</math>0.41</u>	84.57 $\pm$ 0.70
NAGphormer	35.39 $\pm$ 0.80	88.06 $\pm$ 0.43	82.02 $\pm$ 0.98
Exphormer	36.45 $\pm$ 1.21	90.57 $\pm$ 0.64	<u>84.68<math>\pm</math>0.77</u>
<b>WaveGC (ours)</b>	<u>38.61<math>\pm</math>0.74</u>	<b>94.81<math>\pm</math>0.42</b>	<b>85.38<math>\pm</math>0.52</b>

### D.6 Hyper-Parameter Sensitivity Analysis

In WaveGC, two key hyper-parameters, namely  $\rho$  and  $J$ , play important roles. The parameter  $\rho$  governs the number of truncated terms for both  $T_i^o$  and  $T_i^e$ , while  $J$  determines the number of scales

$s_j$  in Eq. (10). In this section, we explore the sensitivity of  $\rho$  and  $J$  on the Peptides-struct (Ps) and Computer datasets. The results are visually presented in Fig.5, where the color depth of each point reflects the corresponding performance (the lighter the color, the better the performance), and the best points are identified with a red star. Observing the results, we note that the optimal value for  $\rho$  is 2 for Ps and 7 for Computer. This discrepancy can be attributed to the substantial difference in the graph sizes between the two datasets, with Computer exhibiting a significantly larger graph size (refer to Appendix D.2). Consequently, a more intricate filter design is necessary for the larger dataset. Concerning  $J$ , the optimal value is determined to be 3 for both Ps and Computer. A too small  $J$  leads to inadequate coverage of ranges, while an excessively large  $J$  results in redundant scales with overlapping ranges.



## D.7 Detailed Descriptions of Base Models

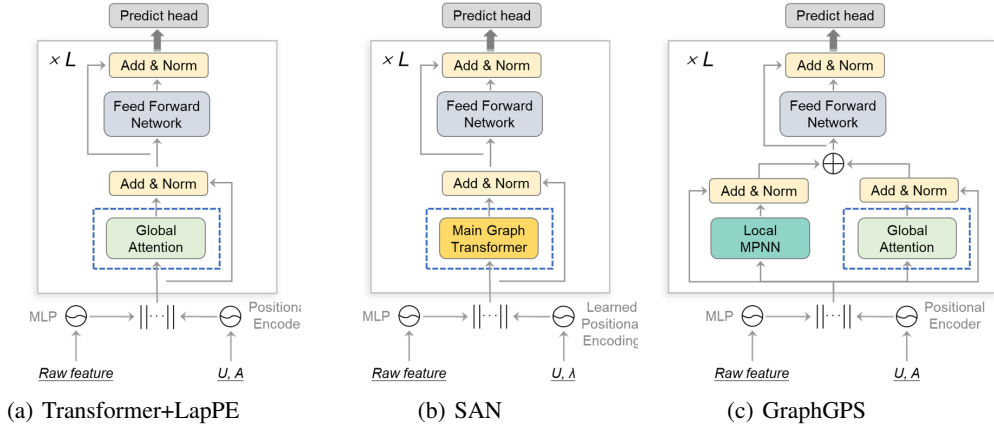


Figure 6: Illustrations of the three base models, including Transformer+LapPE, SAN and GraphGPS. The component surrounded by blue dash line is the part that will be replaced by WaveGC.

As introduced in experiments, we choose three base models, including Transformer [54], SAN [32] and GraphGPS [47], and then replace the Transformer component with our WaveGC for each model, to roundly verify the effectiveness of WaveGC. Therefore, it is necessary to briefly introduce their mechanisms in this section. The illustrations of these three methods are given in Fig. 6.

- **Transformer.** In Fig. 6(a), we show the case that the first several eigenvectors are regarded as positional encoding for each node, denoted as LapPE. During the training, the sign of these eigenvectors is frequently flipped to manipulate the model to avoid the influence from the original sign. Then, this positional encoding is concatenated with raw feature after projection, and input to a vanilla Transformer (Global Attention). The output of Transformer will be combined with its input, and pass through two-layers MLP (Feed Forward Network). After another skip-connection and normalization, we finish one layer of Transformer. In traditional settings, this process will loop several times.

- **SAN.** As shown in Fig. 6(b), SAN proposes some special designs for both positional encoding and Transformer. For the former, Learned positional encoding (LPE) architecture is given. Specifically, for some node  $i$ , the authors concatenate the eigenvalues and  $i$ th entry in each normalized eigenvector, then they use linear layer to mix eigenvalues and eigenvectors, and then a Transformer encoder is utilized to mix different channels. Finally, a sum pooling layer is utilized to get the final LPE for each node. For the latter, similar to Transformer, the authors additionally consider the effect of edge feature when calculating attention values. To emphasize the importance of local structure, they assign different weights to neighbor nodes and distant nodes.
- **GraphGPS.** The aim of this work is to build a general, powerful, scalable graph Transformer with linear complexity as shown in Fig. 6(c). Besides the global attention part, they explicitly involve a parallel MPNN to encode the given topological structure. Then, these two branches separately go through skip-connection and normalization, and then sum together followed by FFN, skip-connection and normalization. For generalization, the authors also provide different choices for positional encoding, local MPNN and Global Attention.

The Global Attention (or Main Graph Transformer) part is surrounded by blue dash line, which is replaced by our WaveGC. Our main target is to boost the base models by this replacement.

## D.8 Hyper-parameters Settings

We implement our WaveGC in PyTorch, and list some important parameter values in our model in Table 15. Please note that for the five long-range datasets, we follow the parameter budget  $\sim 500k$  [14].

Table 15: The values of parameters used in WaveGC (T: True; F: False).

Method	Dataset	# parameters	$\rho$	$J$	$\bar{s}$	Tight frames	Parameters sharing	$\aleph$
Transformer +WaveGC	CS	437k	3	3	{0.5, 0.5, 0.5}	T	T	0.1
	Photo	122k	3	3	{1.0, 1.0, 1.0}	T	T	0.1
	Computer	150k	7	3	{1.0, 1.0, 1.0}	T	T	0.1
	CoraFull	547k	3	3	{2.0, 2.0, 2.0}	T	T	0.1
	ogbn-arxiv	2,091k	3	3	{0.1, 0.8, 5.0}	F	T	0.03
	PascalVOC-SP	477k	3	3	{0.5, 1.0, 10.0}	T	F	/
	PCQM-Contact	480k	5	3	{0.5, 1.0, 5.0}	T	F	/
	COCO-SP	553k	3	3	{10.0, 10.0, 10.0}	T	T	/
	Peptides-func	467k	5	3	{10.0, 10.0, 10.0}	T	T	/
	Peptides-struct	534k	2	3	{0.3, 1.0, 10.0}	F	F	/
SAN +WaveGC	CS	524k	3	3	{0.5, 0.5, 0.5}	T	T	0.1
	Photo	262k	3	3	{1.0, 1.0, 1.0}	T	T	0.01
	Computer	292k	3	3	{2.0, 2.0, 2.0}	T	T	0.1
	CoraFull	619k	3	2	{2.0, 2.0}	T	T	0.1
	ogbn-arxiv	2,352k	3	3	{0.1, 0.8, 5.0}	F	T	0.03
	PascalVOC-SP	464k	3	3	{0.5, 1.0, 10.0}	T	F	/
	PCQM-Contact	411k	3	3	{0.5, 1.0, 5.0}	T	F	/
	COCO-SP	469k	3	3	{10.0, 10.0, 10.0}	T	T	/
	Peptides-func	405k	5	3	{10.0, 10.0, 10.0}	T	T	/
	Peptides-struct	406k	3	3	{0.3, 1.0, 10.0}	T	F	/
GraphGPS +WaveGC	CS	495k	3	3	{0.5, 0.5, 0.5}	T	T	0.1
	Photo	136k	3	3	{1.0, 1.0, 1.0}	T	T	0.1
	Computer	167k	3	3	{1.0, 1.0, 1.0}	T	T	0.1
	CoraFull	621k	3	3	{2.0, 2.0, 2.0}	T	T	0.1
	ogbn-arxiv	2,354k	3	3	{0.1, 0.8, 5.0}	F	T	0.03
	PascalVOC-SP	506k	5	3	{0.5, 1.0, 10.0}	T	F	/
	PCQM-Contact	508k	5	3	{0.5, 1.0, 5.0}	T	F	/
	COCO-SP	546k	3	3	{0.5, 1.0, 10.0}	T	F	/
	Peptides-func	496k	5	3	{10.0, 10.0, 10.0}	T	T	/
	Peptides-struct	534k	3	3	{0.3, 1.0, 10.0}	F	F	/

## D.9 Operating Environment

The environment where our code runs is shown as follows:

- Operating system: Linux version 5.11.0-43-generic

- CPU information: Intel(R) Xeon(R) Gold 6226R CPU @ 2.90GHz
- GPU information: NVIDIA RTX A5000

## E Related Work

**Graph Transformer.** Graph Transformer (GT) has attracted considerable attentions, where researchers mainly focus on two aspects, i.e., positional encoding and reduction of computational complexity. Firstly, a suitable positional encoding (PE) can assist the Transformer to understand the topology and complex relationships within the graph. GT [13] proposes to employ Laplacian eigenvectors as PE with randomly flipping their signs. Graphormer [64] takes the distance of the shortest path between two nodes as spatial encoding, which is involved in attention calculation as a bias. SAN [32] conducts a learned positional encoding architecture to address key limitations of previous GT analyzed in the paper. GraphGPS [47] provides different choices for PE, consisting of LapPE, RWSE, SignNet and EquivStableLapPE. GRIT [41] uses the proposed relative random walk probabilities (RRWP) initial PE to incorporate graph inductive biases. [17] proposes two direction- and structure-aware PE for directed graphs, i.e., Magnetic Laplacian and directional random walk encoding. Both GraphTrans [60] and SAT [6] adopts a GNN cascaded with Transformer, where GNN can be viewed as an implicit PE to capture the local structure. Secondly, because of the huge complexity of attention computation  $O(N^2)$ , some studies endeavor to reduce it to the linear complexity. ANS-GT [65] proposes a hierarchical attention scheme with graph coarsening. DIFFORMER [58] introduces an energy constrained diffusion model with a linear-complexity version. EXPHORMER [50] consists of a sparse attention mechanism based on virtual global nodes and expander graphs. NAGphormer [7] can be trained in a mini-batch manner by aggregating neighbors from different hops with Hop2Token. NodeFormer [57] enables the efficient computation via kernelized Gumbel-Softmax operator. SGFormer [59] is empowered by a simple attention model that can efficiently propagate information among arbitrary nodes. Besides these two main aspects, Edgeformers [29] and EGT [27] additionally explore the edges by injecting edge text information or designing residual edge channels respectively. Furthermore, BRAIN NETWORK TRANSFORMER [30] and Grover [48] explore the applications of GT on human brains and molecular data.

**Graph Wavelet Transform.** Graph wavelet transform is a generalization of classical wavelet transform [42] into graph domain. SGWT [20] defines the computing paradigm on weighted graph via spectral graph theory. Specifically, it defines scaling operation in time field as the scaling on eigenvalues. The authors also prove the localization properties of SGWT in the spatial domain in the limit of fine scales. To accelerate the computation on transform, they additionally present a fast Chebyshev polynomial approximation algorithm. Following SGWT, there have been some efforts on designing more powerful graph wavelet bases in spectral domain, whereas these methods have different flaws. GWNN [61] chooses heat kernel as the filter to construct the bases. SGWF [49] proposes an end-to-end learned kernel function using MLP. LGWNN [63] designs neural network-parameterized lifting structures, where the lifting operation is based on diffusion wavelets. The graph wavelet bases learnt from these three methods are not guaranteed as band-pass filters in  $\lambda \in [0, 2]$  and thus violate admissibility condition [42]. UFGCONV [66] defines a framelet-based graph convolution with Haar-type filters. Wave-GD [9] focuses on graph generation with score-based diffusion, and realizes multiple resolutions with graph wavelet. Furthermore, the authors set  $k(s) = sx e^{-sx}$  as band-pass filter and  $k(s) = e^{-sx}$  as low-pass filter. The above two methods fix the form of the constructed wavelets, extremely limiting the adaptivity to different datasets. In this paper, our WaveGC constructs band-pass filter and low-pass filter purely depending on the even terms and odd terms of Chebyshev polynomials. In this case, the admissibility condition is strictly guaranteed, and the constructed graph wavelets can be arbitrarily complex and flexible with the number of truncated terms increasing. In addition, there are also some papers exploring the applications of graph wavelets on multi-resolution matrix factorization [28] and tensor decomposition [36].